Cell

Facile discovery of surrogate cytokine agonists

Graphical abstract

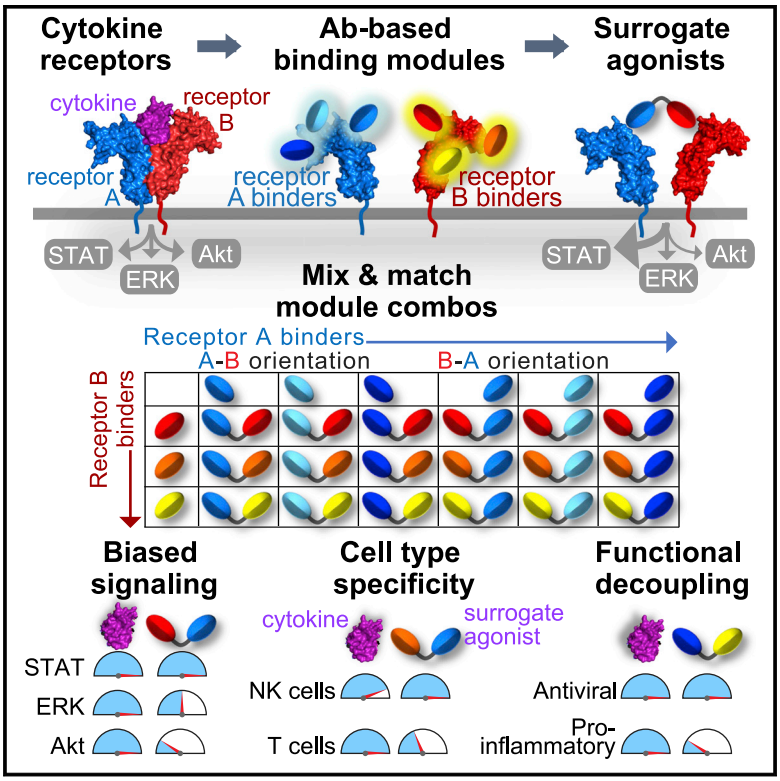

Highlights

- A platform to expand and diversify cytokine biology with modular surrogate agonists
- IL-2 surrogates reveal signaling plasticity and biased activities on T and NK cells
- Type-I IFN surrogates are potent antiviral agents with reduced cytotoxic properties
- IL-2/10 surrogates drive non-natural receptor hetero-dimerization on T and NK cells

Authors

Michelle Yen, Junming Ren, Qingxiang Liu, ..., Ralph S. Baric, Leon L. Su, K. Christopher Garcia

Correspondence

kcgarcia@stanford.edu

In brief

A discovery platform for functionally diverse cytokine surrogates.

Yen et al., 2022, Cell *185*, 1–17
April 14, 2022
https://doi.org/10.1016/j.cell.2022.02.025

Cell

CellPress

Article

Facile discovery of surrogate cytokine agonists

Michelle Yen,[1,2,6] Junming Ren,[1,2,6] Qingxiang Liu,[1,2,6] Caleb R. Glassman,[1,2] Timothy P. Sheahan,[3] Lora K. Picton,[1,2] Fernando R. Moreira,[3] Arjun Rustagi,[4] Kevin M. Jude,[1,2] Xiang Zhao,[1,2] Catherine A. Blish,[4,5] Ralph S. Baric,[3] Leon L. Su,[1,2] and K. Christopher Garcia[1,2,7,*]

[1]Departments of Molecular and Cellular Physiology, and Structural Biology, Stanford University School of Medicine, Stanford, CA 94305, USA
[2]Howard Hughes Medical Institute, Stanford University School of Medicine, Stanford, CA 94305, USA
[3]Department of Epidemiology, Gillings School of Global Public Health, University of North Carolina at Chapel Hill, Chapel Hill, NC 27599, USA
[4]Department of Medicine, Stanford University School of Medicine, Stanford, CA 94305, USA
[5]Chan Zuckerberg Biohub, San Francisco, CA 94158, USA
[6]These authors contributed equally
[7]Lead contact
*Correspondence: kcgarcia@stanford.edu
https://doi.org/10.1016/j.cell.2022.02.025

SUMMARY

Cytokines are powerful immune modulators that initiate signaling through receptor dimerization, but natural cytokines have structural limitations as therapeutics. We present a strategy to discover cytokine surrogate agonists by using modular ligands that exploit induced proximity and receptor dimer geometry as pharmacological metrics amenable to high-throughput screening. Using VHH and scFv to human interleukin-2/15, type-I interferon, and interleukin-10 receptors, we generated combinatorial matrices of single-chain bispecific ligands that exhibited diverse spectrums of functional activities, including potent inhibition of SARS-CoV-2 by surrogate interferons. Crystal structures of IL-2R:VHH complexes revealed that variation in receptor dimer geometries resulted in functionally diverse signaling outputs. This modular platform enabled engineering of surrogate ligands that compelled assembly of an IL-2R/IL-10R heterodimer, which does not naturally exist, that signaled through pSTAT5 on T and natural killer (NK) cells. This "cytokine med-chem" approach, rooted in principles of induced proximity, is generalizable for discovery of diversified agonists for many ligand-receptor systems.

INTRODUCTION

Cytokines are garnering increasing interest as therapeutics. However, the process of therapeutic cytokine discovery is generally limited to exploring intrinsic biological properties of natural ligands, through modifications such as affinity maturation, half-life extension and/or tissue targeting (Berraondo et al., 2019; Mansurov et al., 2021; Overwijk et al., 2021). More recently, cytokine engineering strategies have succeeded in demonstrating that cytokine pleiotropy can be mitigated by selective structure-based engineering and protein design (Levin et al., 2012; Glassman et al., 2021b; Mendoza et al., 2019; Mitra et al., 2015; Glassman et al., 2021a; Saxton et al., 2021). However, unlike multi-pass transmembrane proteins such as GPCRs and ion channels that are responsive to small molecule agonists (Shoichet and Kobilka, 2012), cytokines are proteins that signal through type-I single-pass transmembrane receptors, which present immense challenges for small molecule agonist discovery. This is due to two principal reasons.

First, cytokines are globular proteins that function to dimerize their receptors via protein-protein interactions with their receptor extracellular domains (Spangler et al., 2015; Stroud and Wells, 2004). In contrast, small molecule agonists bind within pockets in G-protein-coupled receptor (GPCR) and ion channel transmembrane helices to activate conformational changes. Thus, because of their structural properties, cytokine and growth factor type-I single-pass transmembrane receptors are generally unsuitable for small-molecule-library-based screening campaigns to discover agonists, with rare exceptions (Corman and Mohammad, 2010). Furthermore, cytokines themselves are single-domain four-helix bundle proteins that present structural limitations for ligand engineering (Silva et al., 2019), which is generally restricted to interface mutagenesis.

Second, cytokine-mediated signaling is often assumed to be "on or off," in contrast to graded, or rheostat-like GPCR (i.e., biased) signaling (Smith et al., 2018). However, recent studies have shown that strategic ligand affinity modulation, as well as the orientation and proximity of dimeric receptor assemblies can profoundly influence signaling output to exhibit rheostat-like behavior in a manner conceptually analogous to GPCRs (Glassman et al., 2021b; Mohan et al., 2019; Moraga et al., 2015; Saxton et al., 2021). Furthermore, antibodies to cytokine receptor ECDs can, in some instances, act as "surrogate" cytokine agonists by dimerizing the cytokine receptors into

Please cite this article in press as: Yen et al., Facile discovery of surrogate cytokine agonists, Cell (2022), https://doi.org/10.1016/j.cell.2022.02.025

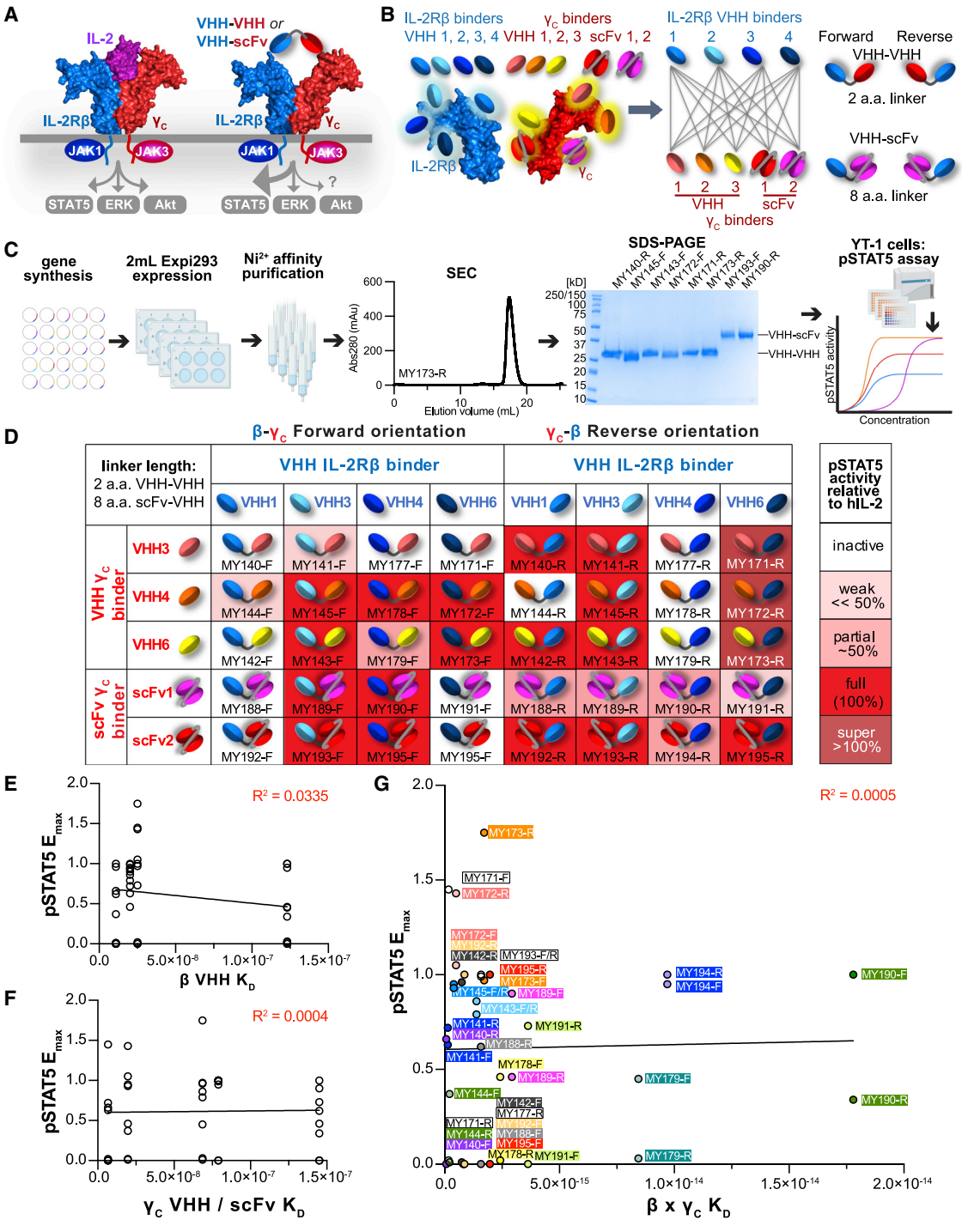

Figure 1. Platform for generation and screening of bispecific IL-2Rβ/γ_C surrogate agonists

(A) Platform for discovery of surrogate IL-2 receptor agonists based on construction of bispecific VHH or scFv specific for IL-2Rβ and γ_C.

(B) Schematic representation of VHH and scFv binding to diverse epitopes along the IL-2Rβ or γ_C extracellular domains (left), combinatorial matrix to generate a collection of β-γ dimerizing ligands (middle), and representation of VHH-VHH or VHH-scFv fusion constructs connected by short linkers in forward or reverse orientations (right).

(C) Schematic pipeline for protein expression and activity screening of surrogate ligands. Bispecific VHH were produced by gene synthesis of VHH monomers and cloning, expressed at 2-mL scale in Expi293 cells and purified via their 6-His tags on Ni^{2+} affinity resin followed by size exclusion chromatography (SEC) and SDS-PAGE analysis. Protein activity was measured via a pSTAT5 phosphoflow assay on YT-1 cells.

(legend continued on next page)

appropriate signaling geometries (Harris et al., 2021; Moraga et al., 2015; Zhang et al., 2013). Taken together, a class of surrogate ligands, with drug-like properties, which can induce varied type-I transmembrane receptor orientations and proximities, and is amenable to high-throughput screening, could bridge the gap between the power of medicinal chemistry and the limitations of cytokine engineering, which does not access the full scope of cytokine receptor signaling plasticity.

In this study, we utilized a receptor-induced proximity strategy to create surrogates of four pleiotropic immunoregulatory cytokines: interleukin-2 and interleukin-15, type-I interferon, and interleukin-10. Interleukin-2 (IL-2) is a stimulatory cytokine that directs proliferation and survival of T lymphocytes, natural killer (NK) cells, and B lymphocytes (Lin and Leonard, 2018). IL-2, similar to IL-15, signals through a receptor heterodimer composed of common gamma (γ_c) and IL-2Rβ, which trigger signaling through JAK-STAT, MAP kinase/ERK, and PI3 kinase-Akt pathways (Leonard et al., 2019). IL-2 activates JAK1 and JAK3 kinases, which relay the signal primarily through STAT5 activity (Miyazaki et al., 1994; Russell et al., 1994; Xue et al., 2002). Type-I interferons (IFNs) have a wide range of immunomodulatory, antiviral, and anti-proliferative actions that are mediated by 16 different sub-types of IFN cytokines that dimerize IFNAR1/IFNAR2 to activate several STATs, principally STAT1. Finally, IL-10 is an anti-inflammatory cytokine that dimerizes IL-10Rα and IL-10Rβ to elicit STAT1 and STAT3 activation (Ouyang and O'Garra, 2019).

We present an unbiased, structurally agonistic, and modular platform for surrogate cytokine discovery which samples the effects of varied receptor dimerization geometries as well as ligand-receptor affinities, on signaling and function of IL-2/15 receptors, type-I IFN receptors, and IL-10 receptors. This led to the discovery of a wide range of functionally diverse ligands, including 28 IL-2 "surrogate" agonists with differing patterns of STAT1/3/5, ERK, and PI3K signaling, preferential induction of memory T cell differentiation, and NK cell cytotoxicity relative to IL-2. IFN surrogate agonists showed biased induction of antiviral genes and potent antiviral activity against SARS-CoV-2. Finally, we demonstrate that surrogate ligands can compel heterodimerization of cytokine receptors for which a natural cytokine ligand does not exist: a surrogate bispecific ligand assembled a "non-natural" signaling entity between IL-2 and IL-10 receptors, resulting in a hybrid signaling entity on NK and $CD8^+$ T cells. Overall, this approach exploits the intrinsic signaling and functional plasticity of cytokines using a scalable and modular strategy for agonist discovery that constitutes a form of "cytokine med-chem" applicable to many cell surface transmembrane receptor systems.

RESULTS

A platform for discovery of bispecific surrogate cytokine agonists

We devised a screening platform consisting of single-chain, bispecific ligands comprised of small antibody domains (VHH and/or scFv) that can be "mixed and matched" in modular fashion to create libraries of dimerizing ligands (Figures 1A and 1B). Using antibody-based binding domains offers the possibility of diverse epitope coverage of the target receptor ECDs, which will manifest as diverse dimerizing topologies in the context of bispecific ligands, in addition to their drug-like properties facilitating clinical translation.

In the IL-2/15 system, we first generated a collection of small, single Ig-domain VHH binders against IL-2Rβ and γ_C selected from phage-displayed libraries of target-immunized Bactrian camels (Figures S1A–S1D). ELISA-based screening of recombinantly expressed VHH clones identified 65 IL-2Rβ binders and 50 γ_C binders. Based on their CDR3 sequence diversity, 10 IL-2Rβ clones from the 4 VHH classes and 6 γ_C clones were selected for further evaluation. The binning into distinct VHH classes was to select for diverse epitope coverage on the receptor ECDs.

We assessed the ability of the isolated VHHs to bind to YT-1 cells, a human NK cell line which endogenously expresses IL-2Rβ and γ_C (Figures S1E–S1H). Four IL-2Rβ-specific VHH clones (β-VHH1, 3, 4, and 6) were chosen for SPR analysis and bound to IL-2Rβ with steady-state affinities ranging from ~10 to 125 nM (Figure S2A). VHH against γ_C were also used for cell-binding studies on YT-1 cells (Figure S1G), and SPR experiments yielded affinities ranging from ~7 to 70 nM (Figure S2B). We selected four IL-2Rβ binders (β-VHH1, 3, 4, and 6), three γ_C clones (γ_C-VHH3, 4, and 6), along with two γ_C scFv clones (P1A3, P2B9) whose sequences we identified in a patent (Figure S1H) (Wang et al., 2016).

We generated bispecific molecules by fusing IL-2Rβ and γ_C binders through short, flexible Gly-Ser linkers (8 aa for VHH-scFv fusions and 2 aa for VHH-VHH fusions) in both forward and reverse orientations (Figure 1B). In total, the "all by all" matrix of 4 IL-2Rβ binders × 5 γ_C binders × 2 orientations resulted in 40 molecules. These small protein constructs (~23–40 kDa) were rapidly produced by gene synthesis, expressed through transient transfection of approximately 2 mL of Expi293 cells and purified via their 6-His tags using small Ni^{2+}-agarose columns (Figure 1C).

The surrogate dimerizing ligands were then rapidly screened in parallel for induction of STAT5 phosphorylation in YT-1 cells (Figures 1D, S2C, and S2D). Of the 40 candidates, we found 28 agonists (~70% "hit rate"), spanning from minimally active (3 ligands), ~1/2 E_{max} relative to hIL-2 (5 ligands), full E_{max} (17

(D) Heatmap of pSTAT5 activity evoked by bispecific antibody pairings. YT-1 cells were stimulated with saturating ligand concentration for 20 min, fixed and permeabilized, then stained with α-STAT5(pY694)-AlexaFluor647 and analyzed via flow cytometry.

(E) Affinity to IL-2Rβ does not predict STAT5 activity. Each circle represents a bispecific molecule, with pSTAT5 E_{max} (normalized to hIL-2) plotted against the affinity of its IL-2Rβ-specific VHH. Data were fit by linear regression, with $R^2 = 0.0335$.

(F) Affinity to γ_C does not predict STAT5 activity. Each circle represents a bispecific molecule, with pSTAT5 E_{max} (normalized to hIL-2) plotted against the affinity of its γ_C-specific VHH or scFv. Data were fit by linear regression, with $R^2 = 0.0004$.

(G) Overall receptor-binding affinity (IL-2Rβ × γ_C K_D) is not predictive of STAT5 activity. Bispecific molecules with identical IL-2Rβ × γ_C antibody usage are depicted in the same color. Data were fit by linear regression, with $R^2 = 0.0005$.

See also Figures S1, S2A, and S2B.

Please cite this article in press as: Yen et al., Facile discovery of surrogate cytokine agonists, Cell (2022), https://doi.org/10.1016/j.cell.2022.02.025

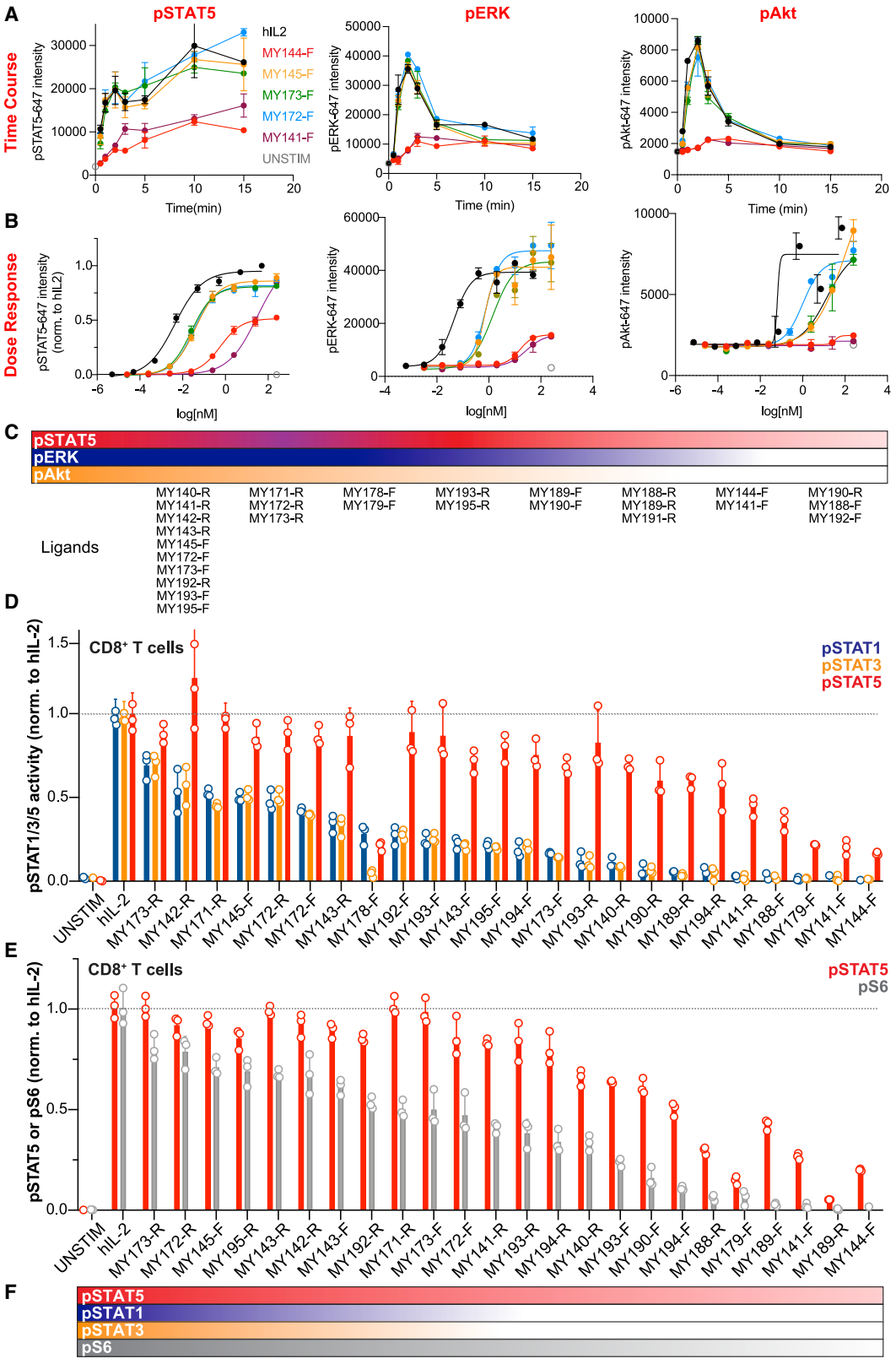

(legend on next page)

Please cite this article in press as: Yen et al., Facile discovery of surrogate cytokine agonists, Cell (2022), https://doi.org/10.1016/j.cell.2022.02.025

ligands), and supraphysiologic E_{max} (3 ligands) (Figures 1D and S2E). Notably, among the agonists, there was no discernable relationship between a ligand's E_{max} and its affinity for individual IL-2Rβ or γ_C receptors (Figures 1E and 1F). This finding highlights the influence of VHH-binding epitope on the receptor ECDs, which influences the overall geometry of the signaling dimer, in addition to ligand-receptor affinity, in determining signaling output. There was also a lack of correlation between E_{max} and the product of receptor-binding affinities β × γ_C (Figure 1G). Even among ligand pairs with identical β and γ_C VHH, alternative (forward or reverse) orientations (β-γ_C versus γ_C-β), elicited divergent activities in 15 of 20 total pairings (Figure 1G).

Profiling signaling properties of IL-2 surrogate ligands

We next examined the principal membrane-proximal outputs of IL-2 signaling: activation of pSTAT5, pERK, and PI3K/pAkt. For kinetics studies, YT-1 cells were stimulated with saturating concentration of hIL-2 or surrogate ligands for varying amounts of time (Figures 2A, S3B, and S3D). For dose-response studies, we varied the concentration of ligand and measured phosphorylation at a fixed time point (3 min) corresponding to peak pERK and pAkt signal levels for hIL-2 (Figures S3A, S3C, and S3E). Surrogate agonists elicited a range of behaviors: some similar to IL-2, while others showed delayed activation and reduced peak responses (MY189-F and MY190-F), and impaired activation of some, but not all pathways (MY178-F, MY179-F) (Figures 2A, 2B, and S3B–S3E). Grouping ligands according to their relative strengths of pSTAT5, pERK, and pAkt signaling (relative to hIL-2) revealed distinct classes of signal patterns (Figure 2C). Across all ligands, pSTAT5 appeared to be preferentially activated, trailed by pERK and then pAkt: pSTAT5 activity ≥ pERK ≥ pAkt.

IL-2 and IL-15 principally activate STAT5 but have also been shown to induce STAT1 and STAT3 activities (Delespine-Carmagnat et al., 2000; Ng and Cantrell, 1997), which are required for efficient maintenance of $CD8^+$ memory T cells (Cui et al., 2011; Quigley et al., 2008; Siegel et al., 2011). We measured STAT1, 3, and 5 phosphorylation after stimulation by IL-2 analogs (Figures S3F and S3G). In pre-activated primary T and NK cells (Figures 2D, S3F, and S3G), ligand MY173-R was similar to IL-2 in its pSTAT1/3/5 balance. However, the remaining surrogate agonists favored dominant pSTAT5 signaling over pSTAT1 and pSTAT3. For example, in $CD8^+$ T cells, MY193-R displayed ~90% pSTAT5 activity, but only ~25% pSTAT1 or pSTAT3 activity relative to hIL-2. We also found that in T cells, many surrogate ligands exhibited higher pSTAT5 activity relative to pS6, a substrate downstream of PI3K/Akt signaling (Ross and Cantrell, 2018) (Figure 2E). In general, the biased pSTAT5 versus pS6 ratio was not as pronounced as in the pSTAT5 versus pSTAT1/3 ratio. In addition to MY173-R (the only ligand with a balanced pSTAT1/3/5 ratio), MY172-R, MY145-F, and MY195-F stimulated balanced levels of pSTAT5 and pS6 phosphorylation in T cells, whereas the remaining ligands favored pSTAT5 activity over pS6 (Figures 2E and 2F).

Surrogate IL-2 ligands form alternative dimeric receptor geometries

To gain insight into the structural basis for signaling differences, we crystalized two different VHHs, one bound to IL-2Rβ and the other bound to γ_C. With structures of the individual receptor:VHH complexes in hand we generated approximate models of the complete dimeric receptor geometry since the short (2 aa) linker places constraints on the relative overall geometry of the two VHHs in the bispecific ligand. The IL-2Rβ:β-VHH6 complex was resolved at 1.9 Å and revealed that the β-VHH6 binds to the D1 domain of the receptor, as opposed to binding at the "elbow" of the D1-D2 juncture like IL-2 (Wang et al., 2005) (Figure 3A; Table S1). We resolved the γ_C:γ_C-VHH6 complex to 2.6 Å and found that the γ_C-VHH6 occupied a similar binding footprint on γ_C as IL-2 (Figure 3B; Table S1). We modeled the two (forward and reverse) orientations of ligands, β-VHH6-γ_C-VHH6 and γ_C-VHH6-β-VHH6. The two complexes predict significant differences from the IL-2 receptor heterodimer geometry in both distance and angular relationship between IL-2Rβ and γ_C (Figures 3C, 3D, and 3E). Surprisingly, we observed that in YT-1 cells γ_C-VHH6-β-VHH6 (MY173-R) induced supraphysiologic STAT5 phosphorylation but normal ERK/Akt phosphorylation relative to hIL-2 (Figures 1D and 2C). The reverse orientation analog, β-VHH6-γ_C-VHH6 (MY173-F), had a similar signaling profile to IL-2 in YT-1 cells. Whereas MY173-R had a signaling profile like IL-2 in $CD8^+$ T and NK cells, MY173-F had high pSTAT5 activity (~70%–100% of IL-2), and low pS6 and pSTAT1/3 activity (50% and ~14%–24%, respectively). These structures support our hypothesis that differences in receptor dimerization geometry strongly influence proximal signaling.

Transcriptional profiling of IL-2 surrogate agonists

We next performed mRNA sequencing to characterize the transcriptional profiles induced by different signaling classes of IL-2

Figure 2. Profiling signaling properties of IL-2 surrogate ligands

(A) Kinetics of pSTAT5, pERK, and pAkt signaling evoked by IL-2 or surrogate agonists. YT-1 cells were serum-starved for 1–2 h, then stimulated with 50-nM ligand for 0.5–15 min at 37°C, fixed and permeabilized, then stained with fluorescently conjugated phospho-antibodies before reading on a flow cytometer. Data were collected in duplicate and displayed as mean ± SD.

(B) Dose-response relationship of pSTAT5, pERK, and pAkt activity evoked by IL-2 or surrogate agonists. Serum-starved YT-1 cells were stimulated with varying concentration of ligand for 3 min, then processed as in (A) for phosphoflow analysis.

(C) Classification of signal strength for IL-2 surrogate agonists, with relative strength of activity encoded by colored gradients.

(D) T cell blasts were stimulated with 50-nM hIL-2 or surrogate agonist for 20 min at 37°C, fixed and permeabilized, then stained with fluorescently conjugated antibodies against pSTAT1, pSTAT3, or pSTAT5 and read on a flow cytometer. Raw fluorescence intensities were background subtracted against that of unstimulated cells, then normalized to hIL-2 values.

(E) T cell blasts were stimulated with 50-nM hIL-2 or surrogate agonist for 1 h at 37°C. Cells were fixed and permeabilized, then stained with fluorescently conjugated antibodies against pSTAT5 and pS6, and read on a flow cytometer. Data are baseline subtracted and normalized as in (D).

(F) Summary of ligand signaling properties across pSTAT1/3/5 and pAkt pathways, with relative strength of activity encoded by colored gradients. Data were collected in triplicate and plotted as mean ± SEM.

See also Figures S2 and S3.

Please cite this article in press as: Yen et al., Facile discovery of surrogate cytokine agonists, Cell (2022), https://doi.org/10.1016/j.cell.2022.02.025

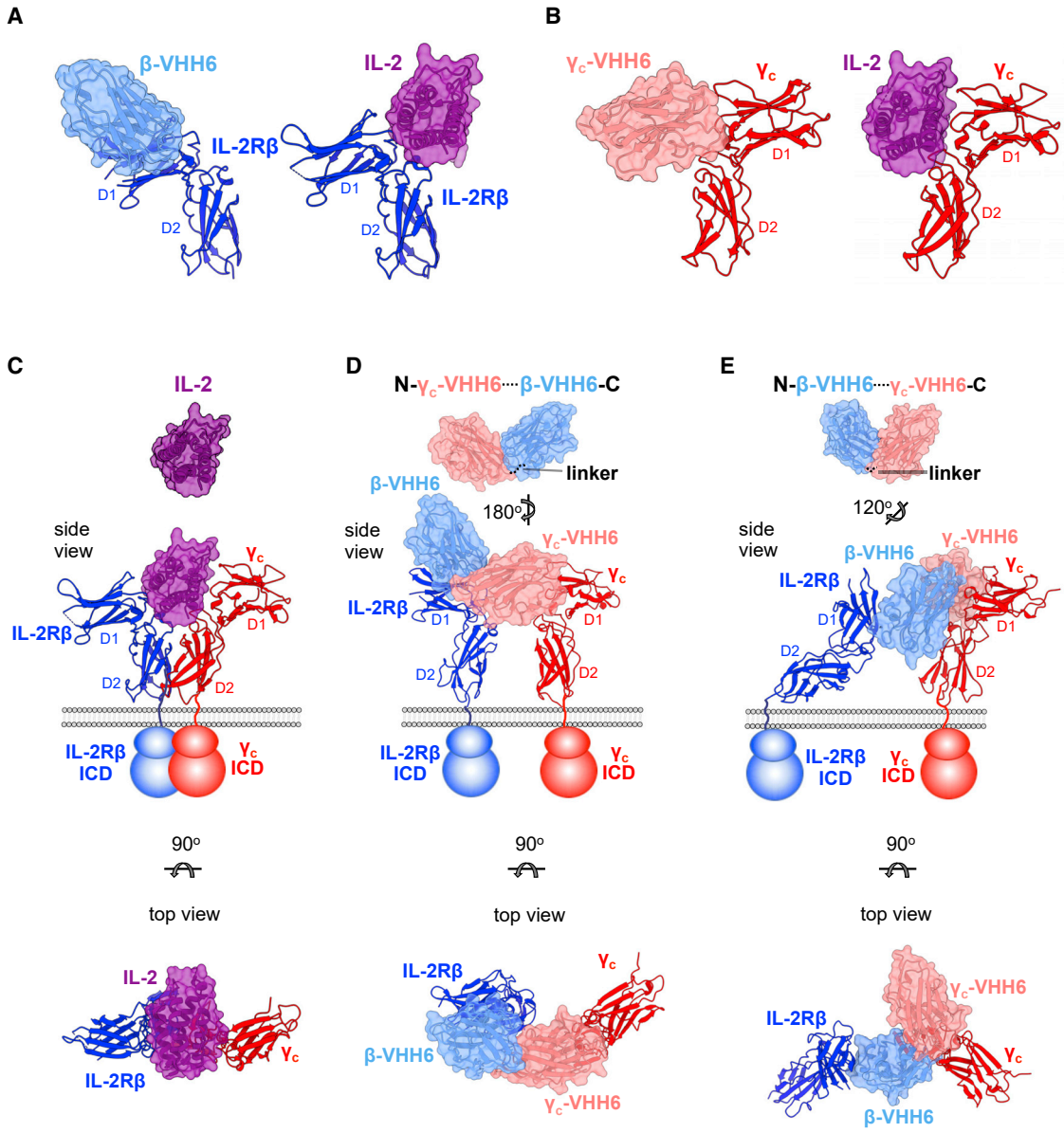

Figure 3. Dimeric geometries from crystal structures of IL-2Rβ:VHH and γ_c:VHH complexes

(A) Sideview comparisons between the human IL-2:IL-2Rβ binary complex (PDB: 2B5I) (Wang et al., 2005) and β-VHH6:IL-2Rβ binary complex. Surface representations of IL-2 and β-VHH6 are colored in purple and light blue, respectively, while IL-2Rβ is shown in ribbon representation in navy.

(B and C) (B) Sideview comparisons of IL-2:γ_C and γ_C-VHH6:γ_C receptor complexes. γ_C-VHH6 is shown in pink, with γ_C colored in red. (C) Crystal structure of the human IL-2:IL-2Rβ:γ_C ternary complex (PDB: 2B5I) (Wang et al., 2005). Sideview with membrane bilayer and schematic representation of receptor transmembrane and intracellular domains (ICD) is shown at middle. Top view (below) is related to the side view by a 90° rotation about the horizontal axis.

(D) Model of γ_C-VHH6-β-VHH6 bound to its receptors. Structures of the γ_C-VHH6:γ_C and IL-2Rβ:β-VHH6 were determined separately. The γ_C-VHH6-β-VHH6 linker distance was modeled in and represented by a dotted line (top), with a side and top views of receptor-bound model shown underneath.

(E) Model of β-VHH6-γ_C-VHH6 bound to its receptors. The VHH-VHH linker was modeled as in (D).

See also Table S1.

surrogate ligands on T cells. Principal component analysis (PCA) indicated that the IL-2 analogs had a concerted effect on gene expression across the PC1 axis (Figure 4A). Within each donor, ligands MY173-R, MY143-R, MY145-F, and MY172-F clustered together with IL-2 and IL-15 (which are known to drive highly similar gene expression profiles; Ring et al., 2012); MY141-F, MY188-R, and MY179-F clustered near the unstimulated sample, whereas MY190-R and MY193-R were close to IL-7, which is required for naive and memory T cell homeostasis and opposes terminal effector T cell differentiation (Shourian et al., 2019) (Figure 4A). These relationships were also preserved on a group level, as seen in the distance calculation matrix

Please cite this article in press as: Yen et al., Facile discovery of surrogate cytokine agonists, Cell (2022), https://doi.org/10.1016/j.cell.2022.02.025

CellPress

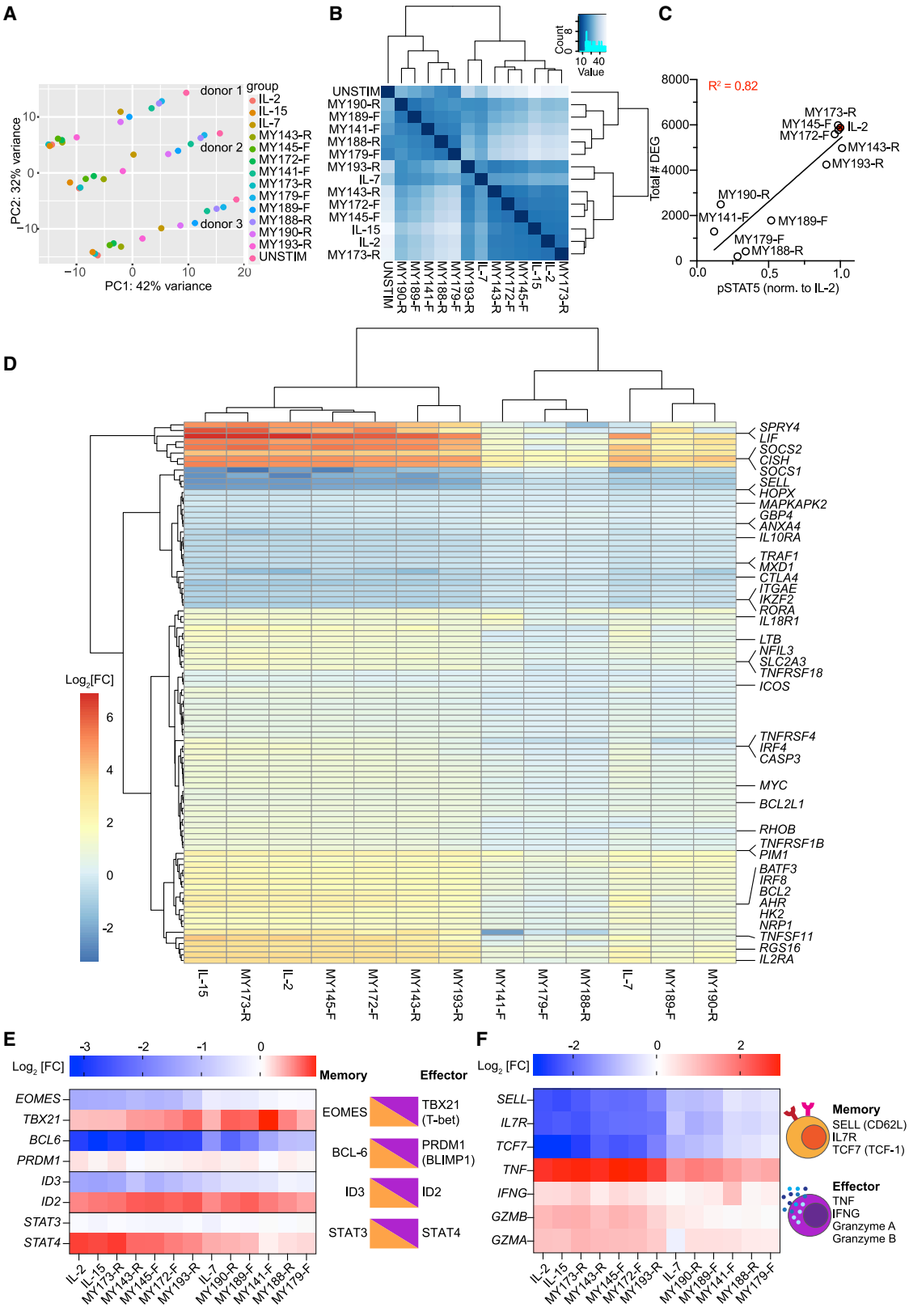

(legend on next page)

Please cite this article in press as: Yen et al., Facile discovery of surrogate cytokine agonists, Cell (2022), https://doi.org/10.1016/j.cell.2022.02.025

(Figure 4B). Overall, a given ligand's pSTAT5 activity (on $CD8^+$ T cells) was linearly correlated with its potency at regulating gene expression (R^2 = 0.82; Figure 4C). We identified 96 STAT5 target genes from a curated gene list (mSigDb) (Liberzon et al., 2015; Subramanian et al., 2005) whose expression was significantly altered by treatment with cytokines or IL-2 analogs ($p_{adj} < 0.05$), including targets known to be highly upregulated by IL-2 (*SOCS1*, *CISH*, *BCL2*, and *IL2RA*). Overall, the IL-2 surrogates regulated STAT5 targets in a graded manner, with strong ligands (MY173-R, MY145-F, MY143-R, and MY172-F) having a similar profile to IL-2 and IL-15, weak ligands (MY141-F, MY179-F, and MY188-R) mildly upregulating robust STAT5 targets such as *SOCS1*, *CISH*, and *SELL*, and having no effect on other targets, and IL-7/MY193-R/MY190-R having an intermediate effect on gene regulation (Figure 4D).

An important function of IL-2 is to induce $CD8^+$ T cell differentiation, so we examined expression of pairs of transcription factors that exert opposing effects on T_{memory} versus $T_{effector}$ differentiation (Kaech and Cui, 2012) (Figure 4E). Four pairs of transcription factors, EOMES/TBX21, BCL-6/PRDM1, ID3/ID2, and STAT3/STAT4, regulate the balance of memory versus effector potential based on their relative expression ratios and/or activities (Kaech and Cui, 2012). We found that along with IL-2/IL-15, ligands MY173-R, MY143-R, MY145-F, and MY172-F downregulated *EOMES* but not *TBX21* and *BCL6* and not *PRDM1*, while upregulating *ID2* but not *ID3*, and *STAT4* but not *STAT3* expression. Taken together these four sets of ratios favor differentiation toward effector over memory cells (Kaech and Cui, 2012). Consistent with this, the same set of ligands downregulated expression of markers of naive and central memory cells (such as *SELL*, *IL7R*, and *TCF7*) while upregulating expression of genes encoding the effector cytokines and cytolytic molecules TNF-α, IFNγ, granzyme A, and granzyme B (Kaech and Cui, 2012) (Figure 4F).

IL-2 surrogate agonists support T and NK cell proliferation and cytolysis

One of the principal roles of IL-2 is to direct the differentiation of naive $CD8^+$ T cells into memory and cytotoxic effector cells; thus, we probed the ability of our ligands to orchestrate development of naive (T_n), central memory (T_{CM}), effector memory (T_{EM}), and more terminally differentiated effector memory CD45RA (T_{EMRA}) T cells (Maecker et al., 2012) (Figures S4A and S4B). Ligands spanned a broad range of differentiation potential, ranging from IL-2-like, to central and effector memory biased, entirely CD8 selective, or nonfunctional despite triggering pSTAT5 signaling (Figures 5A, 5B, and 5D).

We also profiled expression of cytokines important for cytolytic function (Figures 5C, S4C, and S4D). Ligands that supported T cell expansion were tightly correlated with acquisition of proliferative and cytotoxic cytokine production (IL-2, TNF-α, and IFNγ). MY173-R supported equivalent T cell proliferation to IL-2, and the resultant cells had a $CD8^+$ memory distribution phenotype (Figures 5A and 5D, top row). However, relative to hIL-2, a higher proportion of MY173-R-cultured cells produced IFNγ, with a lower proportion making IL-2 and TNF-α (Figure 5C). Another differentiation phenotype is represented by MY173-F and MY193-R. These ligands evoked relatively high levels of pSTAT5 activity (~70%–90% of IL-2) but had lower levels of pSTAT1/3 activity (<30% of hIL-2; Figure 2D) and promoted lower levels of proliferation as compared with hIL-2 (Figure 5D, middle row). Relative to IL-2 treatment, MY173-F and MY193-R drove higher proportions of central memory cells in addition to supporting effector memory differentiation, while inducing less T_{EMRA} cells. A higher fraction of MY193-R-treated cells produced IL-2 with a lower percentage of TNF-α producers, consistent with a central memory phenotype (Figure 5C). A third category of ligands, which includes MY141-F, were strongly central memory dominant (Figure 5D, bottom row).

One clear IL-2-dependent functional readout is cytolysis of target cells. To test this, we used pre-activated human T cells transduced with the A3A T cell receptor (TCR), which recognizes the MAGE-3A peptide presented by HLA-A*01 on A375 melanoma cells (Cameron et al., 2013; Linette et al., 2013). The IL-2 surrogate ligands supported T cell cytotoxic function to varying degrees, largely matching their ability to support $CD8^+$ T cell proliferation and generate effector cytokines (Figure 5G).

IL-2 and IL-15 are also known to support NK cell expansion and arm them with cytotoxic function (Wu et al., 2017). To assess proliferation, we expanded PBMCs with 100-nM hIL-2 or IL-2 surrogates for 14 days, then profiled T and NK cell types using surface antibody staining (Figures 5E and S5A). Culture with

Figure 4. Transcriptional profiling of IL-2 surrogate agonists

(A) Principal component analysis (PCA) of gene expression in $CD8^+$ T cells from 3 donors stimulated with IL-2 or surrogate ligands for 24 h. Samples from a given donor lie along a horizontal line, with unstimulated samples at the right and IL-2/IL-15 treated samples at the left. The effect of various ligand stimulations is largely described by PC1.

(B) Euclidean distance matrix showing overall similarities in mRNA expression between treatment conditions. Samples within the same treatment condition were pooled together. Dendrograms depict the results of unsupervised hierarchical clustering between samples, with the branch length being proportional to the distance between samples.

(C) Relationship between surrogate ligand pSTAT5 activity and the total number of differentially expressed genes (DEGs) induced by ligand stimulation. STAT5 phosphorylation was normalized to that of hIL-2 stimulated cells.

(D) Hierarchical clustering of "Hallmark" STAT5 targets (curated by mSigDB) (Liberzon et al., 2015; Subramanian et al., 2005) whose expression was significantly altered by treatment cytokine or surrogate agonist treatment ($p_{adj} < 0.05$). Differential gene expression is represented as the $\log_2$ fold change (Log_2[FC]) of normalized mRNA counts. Genes are arrayed by row and ligands by column.

(E) Log_2 fold expression change of transcription factors which play opposing roles in $CD8^+$ memory versus effector differentiation. Opposing transcription factor pairs are diagrammed (right) with the accompanying $\log_2$ fold changes induced by surrogate ligands (left).

(F) Log_2 fold expression change of selected markers of memory and effector T cells (left). Memory T cells express CD62L (encoded by SELL), IL7 receptor, and the transcription factor TCF1 (encoded by TCF7), whereas effector $CD8^+$ T cells produce abundant amounts of cytokines TNF-α and IFNγ and cytolytic molecules such as granzymes A and B (right).

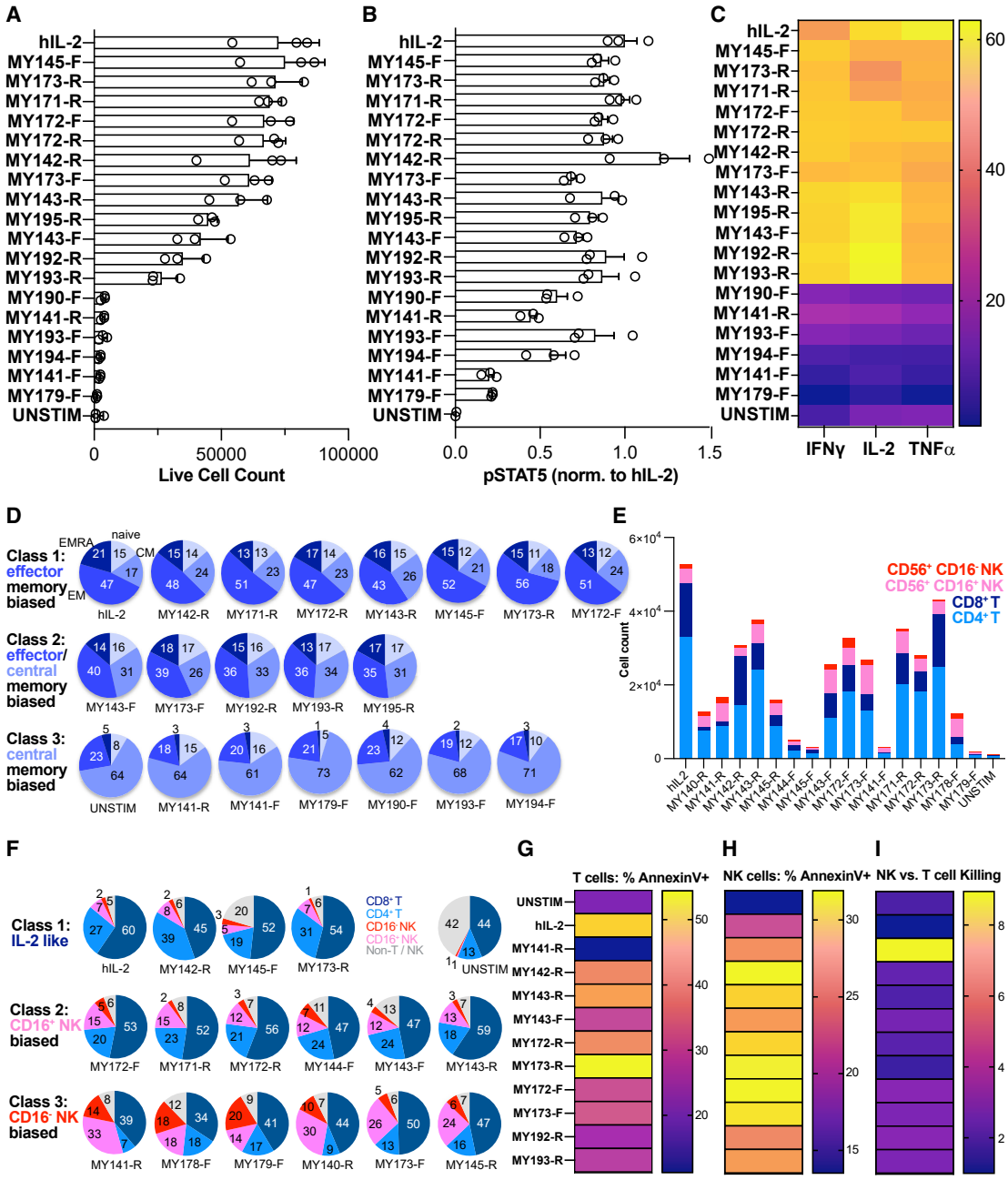

Figure 5. IL-2 surrogate agonists support T and NK cell proliferation and cytolysis

Naive T cells were isolated from PBMC by negative magnetic selection, pre-activated for 4 days with surface-bound α-CD3 + soluble α-CD28, then cultured in the presence of 100-nM hIL-2 or surrogate agonist for 8 days.

(A) Total T cell count after differentiation in the presence of indicated ligand. Wells were set up in triplicate, and data are displayed as mean ± SEM.

(B) pSTAT5 activity in pre-activated T cells, normalized to that of hIL-2.

(C) Cytokine profiling of $CD8^+$ T cells was performed by stimulating cells with PMA + ionomycin in the presence of brefeldin A and monensin, followed by intracellular staining to assess IFNγ, IL-2, and TNF-α production. Data represent an average of 3 replicate wells and are colored by heatmap encoding the percentage of $CD8^+$ cells expressing the indicated cytokine.

(D) Cells were stained with surface antibodies against CD4, CD8, CCR7, and CD45RA to enumerate differentiation into T cell memory sub-types. The fraction of naive, central memory, effector memory, and T_{EMRA} cells are represented using pie charts.

(E) PBMC were cultured for 2 weeks in the presence of 100-nM hIL-2 or surrogate agonists, then stained with phenotyping markers for T and NK cells and enumerated using flow cytometry. The graph displays absolute live cell counts of $CD8^+$ T, $CD4^+$ T, $CD16^+$ NK, and $CD16^-$ NK cells.

(F) Pie charts of cell count data from (E) depict the fraction of T and NK cell types.

(legend continued on next page)

Please cite this article in press as: Yen et al., Facile discovery of surrogate cytokine agonists, Cell (2022), https://doi.org/10.1016/j.cell.2022.02.025

IL-2 supported the highest level of total cell expansion, while 12 of the surrogate agonists increased the proportion of NK cells in the population relative to IL-2-treated cells (Figure 5F), indicating an NK bias. Ligands which supported 24%–50% of total cell number produced an expanded fraction of $CD16^+$ NK cells (~3- to 5-fold increased relative to IL-2), which marks cytolytic NK cells (Cooper et al., 2001). Ligands MY141-R and MY178-F produced 7- and 9-fold expanded fractions of $CD16^-$ NK cells, which are thought to be specialized for cytokine production (Cooper et al., 2001).

We also directly measured the cytotoxic capacity of NK cells cultured with IL-2 or analogs. Surprisingly, a subset of IL-2 surrogate agonists including MY173-R and MY173-F supported annexin positivity rates that were ~23%–45% higher than that produced by IL-2 or IL-15 (Figures 5H and S5B–S5D). The NK versus T cell bias in cell expansion and survival (Figure 5F) suggested that the surrogate ligands might also preferentially drive the ability of NK cells to acquire cytotoxicity over that of T cells. To measure this, we normalized cytotoxicity values for surrogate ligands to that of hIL-2 in NK cells and in T cells, then plotted the normalized NK-to-T cell killing ratio (Figure 5I). Our IL-2 analogs all exhibited bias toward NK-mediated killing (ratio > 1), from slight NK bias (MY173-R, ratio = ~1.4) to moderate (most ligands, including MY173-F, ratio ~2–3) to highly NK selective (MY141-R, ratio ~9).

Type-I IFN surrogate agonists exhibit biased signaling and inhibit viral replication

We applied a similar strategy to create surrogate agonists in the type-I IFN system using a collection of VHH and scFv binders to human IFNAR1 and IFNAR2, fused via 2 or 5 aa linkers (Figures 6A, S6A, and S6B). A subset of binders were selected for SPR analysis and bound to their corresponding receptor with K_D < 1 nM (Figures S6A and S6B). Despite their high affinities, an initial 60-member screening matrix (10 IFNAR1 binders × 6 IFNAR2 binders) in the IFNAR1-IFNAR2 orientation produced only 12 active hits (20% hit rate; Figure 6A). These 12 hits were then expressed in the reverse (IFNAR2-IFNAR1) orientation and screened, and all of them were inactive. A subset of active molecules, which we term "human interferon surrogates" (HISs) 1–7, were selected for further studies (Figure 6A). The HIS ligands induced dose-dependent pSTAT1 activation, the hallmark STAT activated by type-I IFNs, on YT-1 and A549 (lung epithelial) cell lines, as well as on human PBMCs, exhibiting partial agonist E_{max} relative to the natural cytokine human IFNω (Figures 6B–6D). Since type-I IFNs also activate additional STATs, we profiled STAT1-STAT6 phosphorylation. We observed reduced pSTAT1 activation relative to IFNω but equivalent pSTAT2 and pSTAT3 activation on both on the NK cell line YT-1 and A549 cells (Figures 6E, 6F, S6C, and S6D). Thus, the surrogate IFN ligands display signaling bias for pSTAT activation relative to human IFNω.

Type-I IFNs are a critical viral defense mechanism, so we asked whether the surrogate ligands exhibited antiviral activity on A549 cells infected with Sendai virus (SeV). All surrogate ligands showed similar inhibition of SeV replication as IFNω, despite their reduced pSTAT1 activation (Figure 6G). The surrogate ligands also inhibited SARS-CoV-2 replication in A549 cells expressing human ACE2 receptor, as measured with an antiviral assay using recombinant SARS-CoV-2 engineered to express nanoluciferase (Hou et al., 2020a) (Figure 6H). After 24-h pretreatment, we observed a potent dose-dependent antiviral effect on SARS-CoV-2 replication. Interestingly, the antiviral potency of HIS agonists varied based on the identity of the IFNAR1 binder. Whereas all 4 ligands using the "3F11" scFv (HIS1-4) exhibited potent antiviral activity, 2/3 ligands with the "A1" VHH (HIS5-7) had poor activity (Figures 6A and 6H). Three HIS ligands were further examined for their ability to inhibit SARS-CoV-2 (Washington 1 strain) replication in primary human airway cells (Figure S6E) (Fulcher et al., 2005; Hou et al., 2020b). HIS2 significantly reduced SARS-CoV-2 titers at 100 pM, and HIS7 reduced viral titers even at 0.01 pM (Figure S6E), indicating that a subset of HIS ligands act as potent antiviral agents on primary cells.

Type-I IFNs exhibit antiviral ability by inducing interferon-stimulated genes (ISGs), and we observed biased induction of ISGs by the surrogate IFN ligands compared with IFNω. Specifically, HIS ligands maintained high levels of antiviral gene expression but induced lower levels of pro-inflammatory and pro-apoptotic gene expression (Figures 6I and S6F). In human primary airway epithelial cells, HIS agonists induced high levels of the antiviral genes *MX1* and *OAS1* with minimal induction of pro-inflammatory genes *CXCL9* and *CXCL10* (Figures 6J and S6G). Moreover, our agonists effectively inhibited SeV replication in PBMCs while barely inducing pro-inflammatory cytokine expression (Figures 6K, 6L, and S6H). Another functional property of type-I IFNs is anti-proliferative activity, and we observed less pro-apoptotic gene induction by the HIS agonists. Consistent with this ISG bias, the HIS did not suppress cell proliferation as much as IFNω in primary airway epithelial cells (Figure 6M). Taken together, these ligands have biased ISG induction, resulting in preserved antiviral activity but restrained anti-proliferative and pro-inflammatory effects. Collectively, these data demonstrate that surrogate IFN agonists are exquisitely potent antiviral agents against SARS-CoV-2 and could be further explored as potential medical countermeasures for COVID-19, as well as for other viruses.

(G) T cell cytolytic activity stimulated by culture with hIL-2 or surrogate agonists. Pre-activated human T cells were lentivirally transduced with A3A TCR and cultured for 10d in the presence of 100 nM hIL-2 or IL-2 surrogate agonists to generate cytotoxic T cells. Cytotoxicity was measured by mixing effector T cells with a fixed number of CTV-labeled A375 melanoma target cells for 4–6 h, then assessing apoptosis via annexin V staining.

(H) NK cytolytic activity stimulated by culture with hIL-2 or surrogate agonists. Pre-activated NK cells were cultured for 4 weeks in the presence of 100-nM hIL-2 or surrogate agonists and mixed with 25,000 CTV-labeled K562 target cells per well. Following 5 h of incubation, cells were stained with annexin V-PE, then analyzed for early apoptosis using flow cytometry.

(I) Relative efficiency of NK versus T cell cytolysis supported by surrogate IL-2 ligands. Annexin V positivity rates were normalized to hIL-2 in NK cells (H) or T cells (G) cultured with surrogate ligands, then ratioed and represented as a heatmap.

See also Figures S4 and S5.

Please cite this article in press as: Yen et al., Facile discovery of surrogate cytokine agonists, Cell (2022), https://doi.org/10.1016/j.cell.2022.02.025

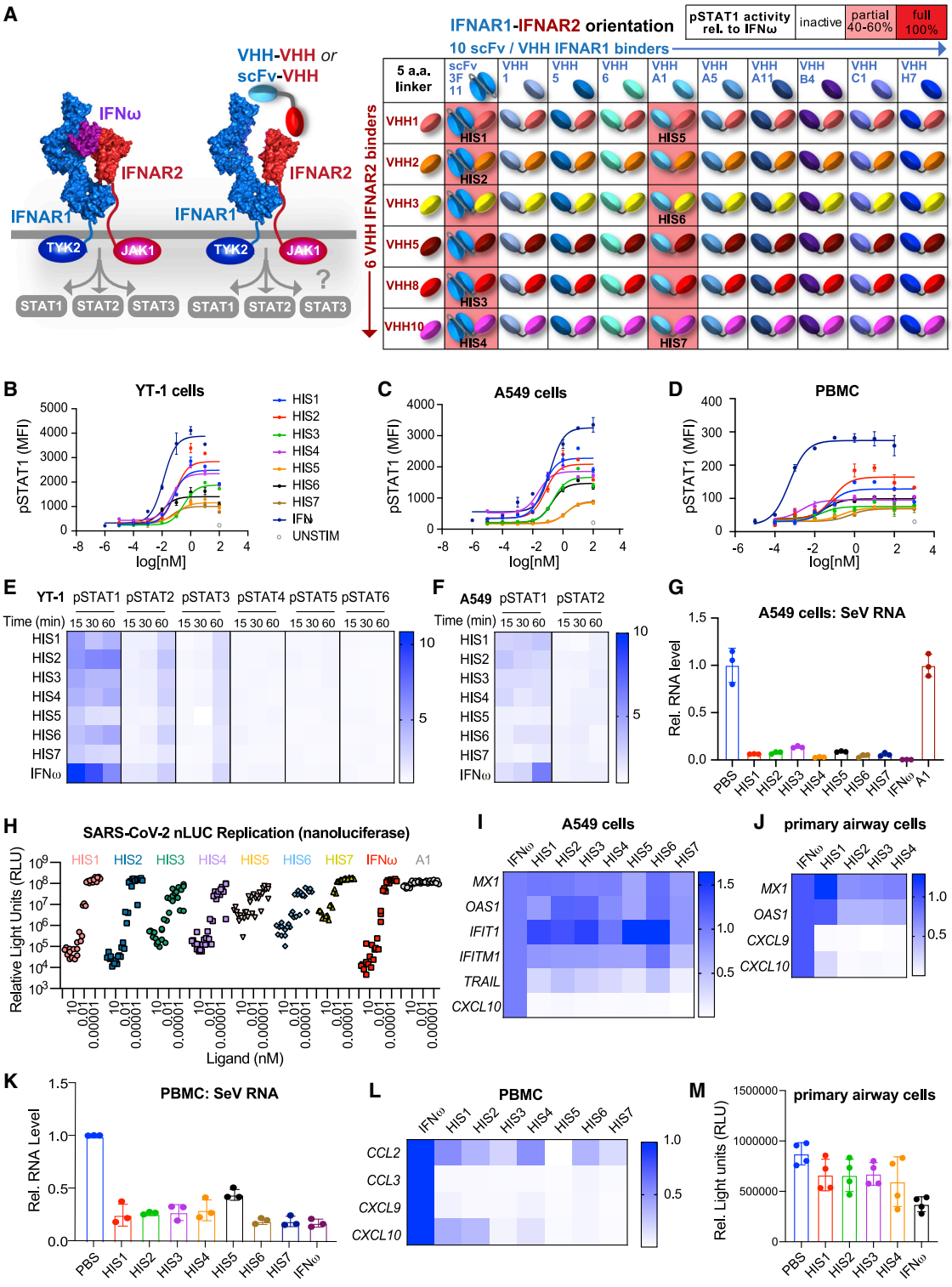

Figure 6. Type-I interferon surrogate agonists exhibit biased signaling and inhibit viral replication

(A) Schematic representation of bispecific type-I IFN surrogate ligands which heterodimerize IFNAR1 and IFNAR2 (left). A collection of 11 IFNAR1 binders (1 scFv, 10 VHH) were paired with 6 IFNAR2 binders (VHH), resulting in 66 combinations of IFNAR1-IFNAR2 fusion molecules connected via a 5 aa linker (right). Twelve of these molecules induced pSTAT1 activity on YT-1 cells (pink shading). The IFNAR2-specific scFv "3F11" was identified from the patent US7662381B2 (Cardarelli et al., 2010). Seven of the hits, "HIS1-7," were selected for further analysis.

(legend continued on next page)

Please cite this article in press as: Yen et al., Facile discovery of surrogate cytokine agonists, Cell (2022), https://doi.org/10.1016/j.cell.2022.02.025

Induced proximity between IL-2Rβ and IL-10Rβ activates pSTAT5 signaling in T and NK cells

The availability of a large collection of VHH and scFv binders to cytokine receptor ECDs enabled us to reach beyond natural pairings of cytokine receptors that are driven by endogenously expressed cytokines, to explore induced proximity of "unnatural" cytokine receptor heterodimer pairs that might elicit non-canonical types of signals. Since IL-2Rβ and IL-10Rβ are co-expressed on T and NK cells, we designed a series of bispecific ligands to induce a "synthetic" IL-2Rβ/IL-10Rβ heterodimer on cells (Figures 7A, S7A, and S7B). In principle, this would create a heterodimeric entity on the cell surface with the potential for JAK1/TYK2 transphosphorylation and activation of pSTAT5 (via IL-2Rβ) and pSTAT3 (via IL-10Rβ). The IL-2Rβ/IL-10Rβ induced proximity approach yielded only 4 active agonist "hits" out of 30 attempted combinations (~13% hit rate; Figure 7B). These ligands showed partial agonism of pSTAT5 relative to hIL-2 (Figure 7B), but none stimulated measurable pSTAT3 activity. One of the most potent, 10Rβ1-2Rβ6, was selected for further optimization by linker length-modulation, which induced pSTAT5 E_{max} activity from very low (16 aa linker) to full agonism equivalent to IL-2 (0 aa linker) and demonstrated the "tunability" of the surrogate system (Figure 7C). We selected the most potent variant, 10Rβ1-2Rβ6 (0 aa) and tested the effect of C-terminal Fc-fusion on pSTAT5 signaling in human primary T cells (Figures 7D and 7E). The Fc-fusion more than doubled the E_{max} relative to the monomeric 10Rβ1-2Rβ6 (Figures 7E and S7C), likely through avidity enhancement.

Given the critical role of STAT5 activity in T cell proliferation, we asked whether the 10Rβ1-2Rβ6 dimerizers could drive primary T cells to proliferate. Monomeric and Fc-linked 10Rβ1-2Rβ6 induced expansion of $CD8^+$ T cells but not $CD4^+$ T cells (Figures 7F and 7G). Stimulation of naive T cells with these ligands in a differentiation assay resulted in a greater fraction of central memory T cells in $CD8^+$ T cells than $CD4^+$ T cells, which is more similar to the actions of IL-7 than to IL-2 (Figure 7H). The 10Rβ1-2Rβ6 and 10Rβ1-2Rβ6-Fc agonists also potentiated $CD8^+$ T cell degranulation (Figure S7D), IFNγ production (Figure S7E), and activation in the A3A-MAGE 3A TCR:pMHC system (Figure S7F). On primary NK cells, 10Rβ1-2Rβ6 and 10Rβ1-2Rβ6-Fc induced different extents of STAT5 phosphorylation (Figure 7I) and proliferation (Figures 7J and S7G). 10Rβ1-2Rβ6 and 10Rβ1-2Rβ6-Fc promoted the lytic activity of NKL cells in a NK cytotoxicity assay against K562 tumor cells and an NK ADCC assay against rituximab-treated Raji tumor cells (Figures 7K and 7L). To assess the effect of these ligands on NK degranulation and activation, we co-cultured NK cells with K562 cells. Treatment with 10Rβ1-2Rβ6 and 10Rβ1-2Rβ6-Fc robustly enhanced CD107 (LAMP-1) surface expression and production of IFNγ and MIP-1β in both primary NK cells or NKL cells (Figures 7M–7O and S7H–S7J, respectively). Our results show that IL-10Rβ/IL-2Rβ agonists preferentially act on $CD8^+$ T cells and NK cells versus IL-2 and that the IL-10Rβ/IL-2Rβ heterodimer signal more closely resembles an IL-2 receptor partial agonist than an IL-10-mediated partial given its pSTAT5 bias.

DISCUSSION

We have exploited the principle of induced proximity of signaling receptors to create a class of modular, surrogate ligands with the capacity to dimerize cell surface receptors in ways that are inaccessible to natural or engineered cytokines. These surrogate agonists have revealed an unexpectedly broad signaling plasticity and functional diversification downstream of these receptors, which can be exploited for drug discovery. The varied and unpredictable structure-activity relationships exhibited by these molecules highlight that the dimeric geometries and proximities of the receptor heterodimers, ligand affinity, and possibly steric effects, are key determinants that collectively modulate signaling in a complex and unpredictable interplay. This strategy is appropriate for dimeric receptor systems with limited or nonexistent structural knowledge (e.g., orphan receptors), or for creating surrogate ligands when the native ligands present biochemical challenges (Janda et al., 2017). Since the binders can be utilized in a pairwise combinatorial manner, the approach can rapidly screen for diverse activities. Unlike combinatorial antibody library-based functional screens (Lerner et al., 2015), our smaller libraries are restricted to modules with biochemically validated binding to the target receptor ECDs so the attribution of agonist activity is unambiguous. In contrast to synthetic chimeric receptor screening systems (Engelowski et al., 2018), our ligands act

(B–D) Dose-response relationship of STAT1 phosphorylation evoked by IFNω or surrogate agonists. YT-1 cells (B), A549 cells (C), or PBMCs (D) were stimulated with saturating ligand concentration for 20 min, fixed and permeabilized, then stained with α-STAT1(pY701)-AlexaFluor647 and analyzed via flow cytometry. Data were collected in duplicate and plotted as mean ± SD.

(E) Heatmap representation of STAT1-STAT6 phosphorylation evoked by surrogate agonists in YT-1 cells at different time points and normalized to the activation induced by IFNω.

(F) Heatmap representation of STAT1 and STAT2 phosphorylation evoked by HIS in A549 cells at varying time points, normalized to activation induced by IFNω.

(G) qRT-PCR analysis of SeV RNA in A549 cells pre-treated with 10 nM HIS or IFNω for 24 h followed by SeV infection (MOI = 0.1) for 24 h.

(H) SARS-CoV-2 nLUC A549-hACE2 antiviral assay. A549-hACE2 cells were treated with varying concentration of HIS, IFNω, or negative control (monomer VHH "A1") for 24 h prior to infection with SARS-CoV-2 nLUC. SARS-CoV-2 nLUC replication (relative light units) for triplicate wells per VHH dilution is shown.

(I and J) Heatmap representation of selected ISGs induced by HIS in A549 cells (I) or human primary bronchial/tracheal epithelial cells (J). Gene expression is normalized to the level induced by IFNω.

(K) qRT-PCR analysis of SeV RNA in PBMCs pre-treated with 10-nM HIS or IFNω for 24 h followed by SeV infection (MOI = 0.5) for 24 h. All qPCR data were collected in triplicate and displayed as mean ± SD in (G) and (K).

(L) Heatmap representation of selected ISGs induced by HIS in PBMCs.

(M) CellTiter-GLO assay of human primary bronchial/tracheal epithelial cells treated with 10 nM HIS or IFNω for 72 h. Data are represented as mean ± SD of triplicate wells.

See also Figure S6.

Please cite this article in press as: Yen et al., Facile discovery of surrogate cytokine agonists, Cell (2022), https://doi.org/10.1016/j.cell.2022.02.025

CellPress

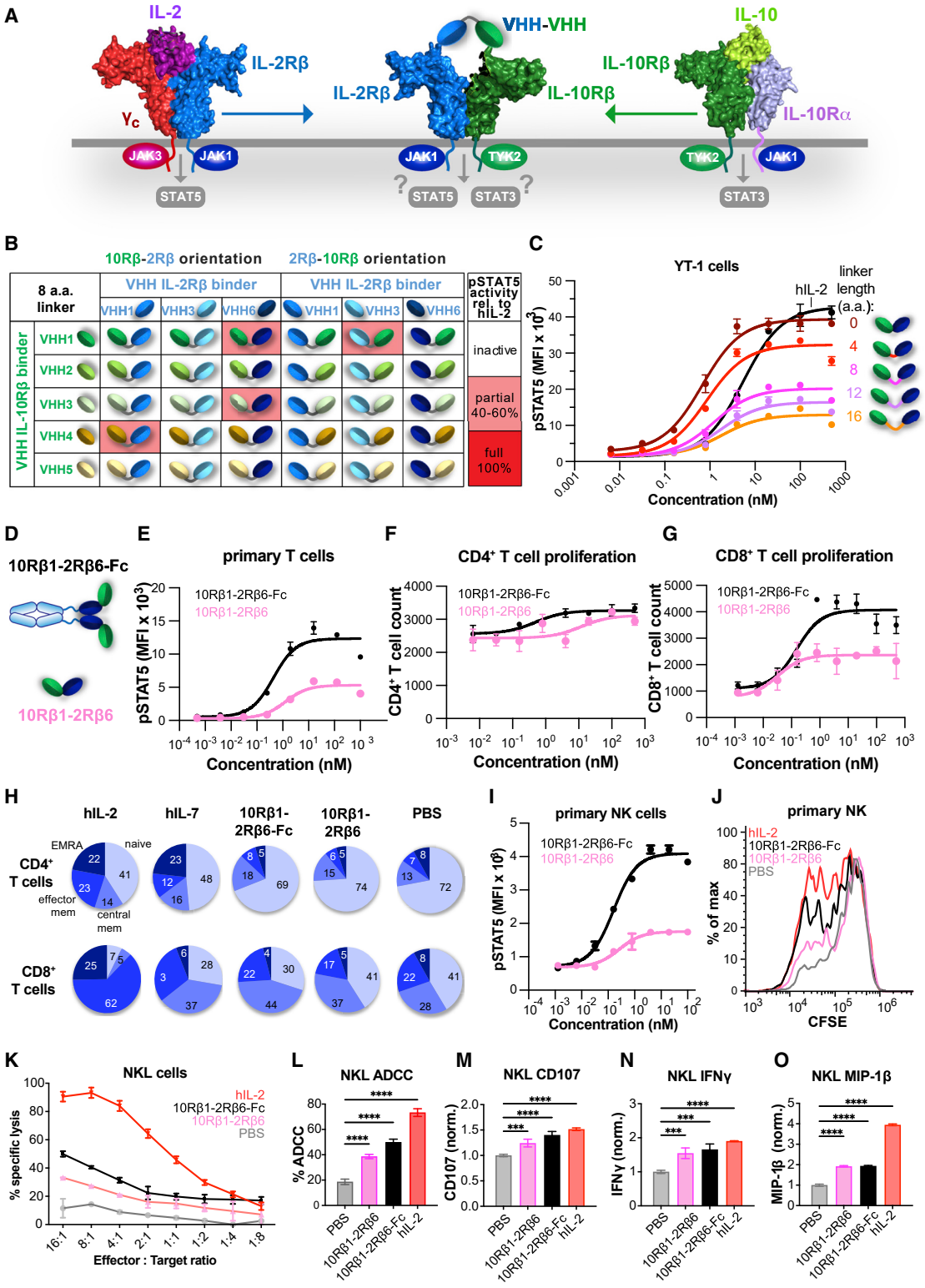

Figure 7. A surrogate agonist that enforces proximity between IL-2Rβ and IL-10Rβ activates pSTAT5 signaling in T and NK cells

(A) Schematic showing non-natural receptor pairing of IL-10Rβ/IL2-Rβ to compel formation of a synthetic JAK1/TYK2 heterodimer.

(B) Thirty IL-10β/IL-2Rβ VHH pairings (with 8 aa linkers) in forward and reverse orientations were expressed and assayed for pSTAT5 activity in YT-1 CD25⁻ cells. Of the thirty combinations, four pairings had partial pSTAT5 activity (pink shading).

(legend continued on next page)

Please cite this article in press as: Yen et al., Facile discovery of surrogate cytokine agonists, Cell (2022), https://doi.org/10.1016/j.cell.2022.02.025

on natural cell types without requiring genetic manipulation. Furthermore, while we fused the modules in a format to create single-chain bispecific ligands that are easily expressed, the approach is also amenable to a vast array of oligomerizing formats and stoichiometries beyond what we describe here. Our modular strategy could be applied toward other dimeric cell surface receptor pairs, such as receptor tyrosine kinase (RTK) systems, BMP, and TGF-β ligand-receptor systems, as well as trimeric death receptors where three, or more, VHHs could be fused. This overall strategy begins to position cytokine, and more broadly, protein-based agonist drug discovery as an induced proximity-based medicinal chemistry platform.

Prior work engineering IL-2 has focused on installing mutations on the natural cytokine scaffold in order to improve its affinity to IL-2Rβ and/or weaken its affinity to γ_C (Glassman et al., 2021a; Levin et al., 2012). Here, our module-based approach allowed us to expand beyond the structural limitations imposed by the cytokine ligand. In comparison with previously reported bispecific antibody IL-2 agonist molecules (Harris et al., 2021), our single-chain platform enables rapid construction, expression, and screening of large libraries and matrices of binders. The surrogate IL-2 analogs we identified enabled us to make several surprising observations about IL-2 signaling. First, we found that the principal signaling pathways downstream of IL-2R engagement—STAT5, ERK, and PI3K-Akt—were not necessarily coupled. ERK and Akt phosphorylation were extremely sensitive to structural perturbation. Whereas ~70% of molecules turned on pSTAT5 activity to some extent, pERK activity was sometimes much weaker or even nonexistent relative to the pSTAT5 amplitude, and pAkt activity was weaker still relative to pERK. These data indicate that signal strength across IL-2 pathways is not intrinsically linked like a rheostat that dials the amplitude in an isotropic manner across pathways, but that pSTAT5 activity may be decoupled from other signals. The differences in proximal signal patterning were manifested in proliferation, differentiation, cytokine secretion, and cytotoxicity. Some ligands exhibited biased abilities to differentiate naive cells into central memory, effector memory, or "exhausted" T cells. Weaker ligands promoted growth only in $CD8^+$ T cells, whereas robust ligands promoted strong central or effector memory phenotypes. Consistent with skewing to effector memory phenotype, these ligands also instructed the resultant T cells to produce cytolytic cytokines and conferred the ability to kill tumor cells.

The endogenous type-I IFN system represents a powerful example of "natural" protein engineering, with 16 cytokine sub-types that signal through a common IFNAR1/IFNAR2 heterodimer, yet elicit differentiated functional effects (Ng et al., 2016; Piehler et al., 2012). This is achieved through polymorphisms within IFN cytokine sub-types that occur at the ligand-receptor interfaces and that lead to different receptor-ligand affinities (Thomas et al., 2011). However, the overall dimeric geometry of the IFNAR1/IFNAR1 heterodimer is very similar among the different IFN sub-types (Thomas et al., 2011), thus the functional differentiation is largely based on differences in cytokine receptor affinity and kinetics (Sandler et al., 2014; Sharma et al., 2016). The surrogate approach takes advantage of the epitope diversity of the VHH and scFv binders on the IFNAR1 and INFAR2 ECDs to achieve further type-I IFN functional diversification. We find that surrogate IFN agonists do not elicit maximal levels of pSTAT1 compared with natural IFN yet exhibit near equivalent antiviral activity against several viruses, including SARS-CoV-2, but reduced expression of pro-inflammatory genes and anti-proliferative activities, two parameters that are thought to contribute to the dose-limiting toxicity of type-I IFNs.

This platform offers additional flexibility to engineer ligands that compel formation of cytokine receptor heterodimers that are not found endogenously. In principle, if two cytokine receptors are expressed on the same cell, the relative promiscuity of JAK and TYK kinases could result in cross-talk and signaling if induced to form heterodimers by a synthetic ligand (Moraga et al., 2017). Here, we have shown that an IL-2Rβ/IL-10Rβ heterodimer generates a pSTAT5 signal that is NK and $CD8^+$ T cell biased and that more resembles an IL-7 signal in its functional effects compared with IL-2, although the investigation of this surrogate cytokine is at an early stage. The differentiated activity of this new signaling entity highlights an unexplored frontier beyond simply recapitulating natural cytokine receptor heterodimers that this platform can fully explore for drug discovery. Beyond JAK/STAT cytokine receptors, crosstalk between unnatural receptor

(C) Modulation of ligand activity by linker length. 10Rβ1-2Rβ6 agonists with varying linker length between 0 and 16 aa were tested for pSTAT5 signaling in YT-1 cells.
(D) Modulation of agonist activity by Fc-mediated dimerization.
(E) Dimerization of the 10Rβ1-2Rβ6 ligand via Fc-fusion enhances pSTAT5 in primary human T cells.
(F and G) $CD8^+$ but not $CD4^+$ T cell proliferation is driven by 10Rβ1-2Rβ6 and 10Rβ1-2Rβ6-Fc. Pre-activated human T cells were cultured with varying concentrations of 10Rβ1-2Rβ6 (pink) and 10Rβ1-2Rβ6-Fc agonists (black). Dose-response relationship of $CD4^+$ (F) and $CD8^+$ (G) T cells proliferation is indicated. Proliferation and pSTAT5 experiments in (B–G) were set up in duplicate, with each point representing the mean ± SD.
(H) $CD8^+$ but not $CD4^+$ T cell differentiation is driven by 10Rβ1-2Rβ6 and 10Rβ1-2Rβ6-Fc.
(I) Dose-response of 10Rβ1-2Rβ6 agonist (pink) and 10Rβ1-2Rβ6-Fc agonist (black) on pSTAT5 in primary effector NK cells. Data (mean ± SD) are from duplicate wells.
(J) Effector NK cells were labeled with 5-μM CFSE for 20 min at 37°C. Histogram at 100-nM ligand concentration displays proliferation of effector NK following 3-day culture.
(K) NKL killing of K562 tumor cells is enhanced by treatment with 10Rβ1-2Rβ6 (pink), 10Rβ1-2Rβ6-Fc (black), and hIL-2 (red). Data were collected in quadruplicate and summarized as mean ± SEM.
(L–O) Degranulation and activation of NKL cells in response to 10Rβ1-2Rβ6, 10Rβ1-2Rβ6-Fc, and hIL-2. Each condition was set up in triplicate and displayed as mean ± SEM. One-way ANOVA followed by Dunnett's multiple comparisons tests was used to calculate statistics, with significance indicated by: ***$p < 0.001$, ****$p<0.0001$.
See also Figure S7.

pairings can be easily explored for other receptor systems using this modular "mix and match" approach.

In the future, this screening platform offers the possibility, with the advent of personalized medicine guided by immune profiling, to reimagine cytokine therapy tailored to bespoke cytokine analogs, chosen from a larger "toolkit" based in individual patient needs. In this sense, cytokine drug discovery will benefit from the indicia of choices that medicinal chemistry has afforded to many classes of small molecule drugs.

Limitations of the study

A limitation of our study is that, while our initial *in vitro* demonstration reveals the creation of a diverse set of cytokine agonists with granular signaling and functional differences, our ability to conduct *in vivo* studies in mouse models was severely limited due to lack of cross-species reactivity of our human receptor-specific VHH and scFv. Future studies will focus on exploring the *in vivo* properties of surrogate agonists either through development of mouse surrogate cytokines or the use of humanized mice.

STAR★METHODS

Detailed methods are provided in the online version of this paper and include the following:

- KEY RESOURCES TABLE
- RESOURCE AVAILABILITY
  - Lead contact
  - Materials availability
  - Data and code availability
- EXPERIMENTAL MODEL AND SUBJECT DETAILS
  - Cell lines and culture conditions for functional studies
  - Cell lines and culture conditions for protein expression
- METHOD DETAILS
  - Camel immunization
  - VHH library construction
  - VHH library selection
  - RNA-seq experiments
  - NK experiments
  - T cell proliferation
  - T cell differentiation
  - Crystallography
  - qRT-PCR
  - Anti-proliferative activity assay
  - A549-hACE2 SARS-CoV-2 antiviral assay
  - SARS-CoV-2 viral inhibition assay
  - NK and NKL functional assays
- QUANTIFICATION AND STATISTICAL ANALYSIS

SUPPLEMENTAL INFORMATION

Supplemental information can be found online at https://doi.org/10.1016/j.cell.2022.02.025.

ACKNOWLEDGMENTS

We acknowledge Yakun Wan for sharing of VHH reagents. This work was supported by National Institute of Allergy and Infectious Diseases (NIAID) grant R37-AI051321 to K.C.G., the Mathers Charitable Foundation, NIAID grants R01 AI132178 and R01 AI132178-04S1 to R.S.B. and T.P.S., and the Bill & Melinda Gates Foundation grant OPP1113682 to C.A.B. This project was supported in part by the North Carolina Policy Collaboratory at University of North Carolina at Chapel Hill, with funding from the North Carolina Coronavirus Relief Fund established and appropriated by the North Carolina General Assembly to R.S.B. K.C.G. is an investigator of the Howard Hughes Medical Institute. M.Y.'s training was supported by the Stanford Immunology Program Training Grant (5T32AI07290-33) and the Stanford Immunology and Rheumatology Training Grant (5T32AR050942-15). A.R.'s training was supported by NIH grant T32 AI007502-23. Use of the Stanford Synchrotron Radiation Lightsource, SLAC National Accelerator Laboratory, is supported by the US Department of Energy, Office of Science, Office of Basic Energy Sciences under contract no. DE-AC02-76SF00515. The SSRL Structural Molecular Biology Program is supported by the DOE Office of Biological and Environmental Research, and by the National Institutes of Health, National Institute of General Medical Sciences (P30GM133894). Portions of schematics in Figures 1C and S4A were generated using BioRender.com.

AUTHOR CONTRIBUTIONS

Conceptualization, K.C.G.; methodology, M.Y., J.R., Q.L., C.R.G., T.P.S., L.K.P., K.M.J., X.Z., C.A.B., R.S.B., and K.C.G.; formal analysis, M.Y., J.R., Q.L., C.R.G., T.P.S., L.K.P., K.M.J., and K.C.G.; investigation, M.Y., J.R., Q.L., C.R.G., T.P.S., L.K.P., F.R.M., A.R., K.M.J., and L.L.S.; writing—original draft, K.C.G., M.Y., and J.R.; writing—review & editing, all authors; visualization, M.Y., J.R., Q.L., C.R.G., T.P.S., L.K.P., and K.M.J.; supervision, K.C.G., R.S.B., and C.A.B.; funding acquisition, K.C.G., R.S.B., T.P.S., and C.A.B.

DECLARATION OF INTERESTS

K.C.G., M.Y., J.R., and Q.L. are co-inventors on a provisional patent 63/306,882 based upon the technology described in this manuscript. K.C.G. is the founder of Synthekine Therapeutics.

Received: October 19, 2021
Revised: January 11, 2022
Accepted: February 22, 2022
Published: March 23, 2022

REFERENCES

Berraondo, P., Sanmamed, M.F., Ochoa, M.C., Etxeberria, I., Aznar, M.A., Pérez-Gracia, J.L., Rodríguez-Ruiz, M.E., Ponz-Sarvise, M., Castañón, E., and Melero, I. (2019). Cytokines in clinical cancer immunotherapy. Br. J. Cancer *120*, 6–15.

Cameron, B.J., Gerry, A.B., Dukes, J., Harper, J.V., Kannan, V., Bianchi, F.C., Grand, F., Brewer, J.E., Gupta, M., Plesa, G., et al. (2013). Identification of a Titin-derived HLA-A1-presented peptide as a cross-reactive target for engineered MAGE A3-directed T cells. Sci. Transl. Med *5*, 197ra103.

Cardarelli, J.M., Witte, A., and Srinivasan, M. (2010). Interferon alpha receptor 1 antibodies and their uses. US Patent 7662381 B2, filed June 20, 2005, and granted February 16, 2010.

Cooper, M.A., Fehniger, T.A., and Caligiuri, M.A. (2001). The biology of human natural killer-cell subsets. Trends Immunol. *22*, 633–640.

Corman, S.L., and Mohammad, R.A. (2010). Eltrombopag: a novel oral thrombopoietin receptor agonist. Ann. Pharmacother. *44*, 1072–1079.

Cui, W., Liu, Y., Weinstein, J.S., Craft, J., and Kaech, S.M. (2011). An interleukin-21-interleukin-10-STAT3 pathway is critical for functional maturation of memory CD8+ T cells. Immunity *35*, 792–805.

Delespine-Carmagnat, M., Bouvier, G., and Bertoglio, J. (2000). Association of STAT1, STAT3 and STAT5 proteins with the IL-2 receptor involves different subdomains of the IL-2 receptor β chain. Eur. J. Immunol. *30*, 59–68.

Emsley, P., Lohkamp, B., Scott, W.G., and Cowtan, K. (2010). Features and development of Coot. Acta Crystallogr. D Biol. Crystallogr. *66*, 486–501.

Engelowski, E., Schneider, A., Franke, M., Xu, H., Clemen, R., Lang, A., Baran, P., Binsch, C., Knebel, B., Al-Hasani, H., et al. (2018). Synthetic cytokine receptors transmit biological signals using artificial ligands. Nat. Commun. *9*, 2034.

Fairhead, M., and Howarth, M. (2015). Site-specific protein labeling: methods and protocols. In Methods in Molecular Biology, A. Gautier and M.J. Hinner, eds. (Springer Science+Business Media), pp. 171–184.

Fulcher, M.L., Gabriel, S., Burns, K.A., Yankaskas, J.R., and Randell, S.H. (2005). Well-differentiated human airway epithelial cell cultures. Methods Mol. Med. *107*, 183–206.

Glassman, C.R., Mathiharan, Y.K., Jude, K.M., Su, L., Panova, O., Lupardus, P.J., Spangler, J.B., Ely, L.K., Thomas, C., Skiniotis, G., and Garcia, K.C. (2021b). Structural basis for IL-12 and IL-23 receptor sharing reveals a gateway for shaping actions on T versus NK cells. Cell *184*, 983–999.e24.

Glassman, C.R., Su, L., Majri-Morrison, S.S., Winkelmann, H., Mo, F., Li, P., Pérez-Cruz, M., Ho, P.P., Koliesnik, I., Nagy, N., et al. (2021a). Calibration of cell-intrinsic interleukin-2 response thresholds guides design of a regulatory T cell biased agonist. eLife *10*, e65777.

Harris, K.E., Lorentsen, K.J., Malik-Chaudhry, H.K., Loughlin, K., Basappa, H.M., Hartstein, S., Ahmil, G., Allen, N.S., Avanzino, B.C., Balasubramani, A., et al. (2021). A bispecific antibody agonist of the IL-2 heterodimeric receptor preferentially promotes in vivo expansion of CD8 and NK cells. Sci. Rep. *11*, 10592.

Hou, Y.J., Chiba, S., Halfmann, P., Ehre, C., Kuroda, M., Dinnon, K.H., Leist, S.R., Schäfer, A., Nakajima, N., Takahashi, K., et al. (2020a). SARS-CoV-2 D614G variant exhibits efficient replication ex vivo and transmission in vivo. Science *370*, 1464–1468.

Hou, Y.J., Okuda, K., Edwards, C.E., Martinez, D.R., Asakura, T., Dinnon, K.H., Kato, T., Lee, R.E., Yount, B.L., Mascenik, T.M., et al. (2020b). SARS-CoV-2 reverse genetics reveals a variable infection gradient in the respiratory tract. Cell *182*, 429–446.e14.

Janda, C.Y., Dang, L.T., You, C., Chang, J., de Lau, W., Zhong, Z.A., Yan, K.S., Marecic, O., Siepe, D., Li, X., et al. (2017). Surrogate Wnt agonists that phenocopy canonical Wnt and β-catenin signalling. Nature *545*, 234–237.

Kabsch, W. (2010). XDS. Acta Crystallogr. D Biol. Crystallogr. *66*, 125–132.

Kaech, S.M., and Cui, W. (2012). Transcriptional control of effector and memory CD8+ T cell differentiation. Nat. Rev. Immunol. *12*, 749–761.

Kromann-Hansen, T., Louise Lange, E., Peter Sørensen, H., Hassanzadeh-Ghassabeh, G., Huang, M., Jensen, J.K., Muyldermans, S., Declerck, P.J., Komives, E.A., and Andreasen, P.A. (2017). Discovery of a novel conformational equilibrium in urokinase-type plasminogen activator. Sci. Rep. *7*, 3385.

Kuziel, W.A., Ju, G., Grdina, T.A., and Greene, W.C. (1993). Unexpected effects of the IL-2 receptor alpha subunit on high affinity IL-2 receptor assembly and function detected with a mutant IL-2 analog. J. Immunol. *150*, 3357–3365.

Leonard, W.J., Lin, J.-X., and O'Shea, J.J. (2019). The γc family of cytokines: basic biology to therapeutic ramifications. Immunity *50*, 832–850.

Lerner, R.A., Grover, R.K., Zhang, H., Xie, J., Han, K.H., Peng, Y., and Yea, K. (2015). Antibodies from combinatorial libraries use functional receptor pleiotropism to regulate cell fates. Q. Rev. Biophys. *48*, 389–394.

Levin, A.M., Bates, D.L., Ring, A.M., Krieg, C., Lin, J.T., Su, L., Moraga, I., Raeber, M.E., Bowman, G.R., Novick, P., et al. (2012). Exploiting a natural conformational switch to engineer an interleukin-2 "superkine.". Nature *484*, 529–533.

Liberzon, A., Birger, C., Thorvaldsdóttir, H., Ghandi, M., Mesirov, J.P., and Tamayo, P. (2015). The Molecular Signatures Database (MSigDB) hallmark gene set collection. Cell Syst. *1*, 417–425.

Liebschner, D., Afonine, P.V., Baker, M.L., Bunkóczi, G., Chen, V.B., Croll, T.I., Hintze, B., Hung, L.W., Jain, S., McCoy, A.J., et al. (2019). Macromolecular structure determination using X-rays, neutrons and electrons: recent developments in Phenix. Acta Crystallogr. D Struct. Biol. *75*, 861–877.

Lin, J.-X., and Leonard, W.J. (2018). The common cytokine receptor γ chain family of cytokines. Cold Spring Harb. Perspect. Biol. *10*, a028449.

Linette, G.P., Stadtmauer, E.A., Maus, M.V., Rapoport, A.P., Levine, B.L., Emery, L., Litzky, L., Bagg, A., Carreno, B.M., Cimino, P.J., et al. (2013). Cardiovascular toxicity and titin cross-reactivity of affinity-enhanced T cells in myeloma and melanoma. Blood *122*, 863–871.

Love, M.I., Huber, W., and Anders, S. (2014). Moderated estimation of fold change and dispersion for RNA-seq data with DESeq2. Genome Biol *15*, 550.

Maecker, H.T., McCoy, J.P., and Nussenblatt, R. (2012). Standardizing immunophenotyping for the Human Immunology Project. Nat. Rev. Immunol. *12*, 191–200.

Mansurov, A., Lauterbach, A., Budina, E., Alpar, A.T., Hubbell, J.A., and Ishihara, J. (2021). Immunoengineering approaches for cytokine therapy. Am. J. Physiol. Cell Physiol. *321*, C369–C383.

Mendoza, J.L., Escalante, N.K., Jude, K.M., Bellon, J.S., Su, L., Horton, T.M., Tsutsumi, N., Berardinelli, S.J., Haltiwanger, R.S., Piehler, J., et al. (2019). Structure of the IFNγ receptor complex guides design of biased agonists. Nature *567*, 56–60.

Mitra, S., Ring, A.M., Amarnath, S., Spangler, J.B., Li, P., Ju, W., Fischer, S., Oh, J., Spolski, R., Weiskopf, K., et al. (2015). Interleukin-2 activity can be fine tuned with engineered receptor signaling clamps. Immunity *42*, 826–838.

Miyazaki, T., Kawahara, A., Fujii, H., Nakagawa, Y., Minami, Y., Liu, Z.J., Oishi, I., Silvennoinen, O., Witthuhn, B.A., and Ihle, J.N. (1994). Functional activation of Jak1 and Jak3 by selective association with IL-2 receptor subunits. Science *266*, 1045–1047.

Mohan, K., Ueda, G., Kim, A.R., Jude, K.M., Fallas, J.A., Guo, Y., Hafer, M., Miao, Y., Saxton, R.A., Piehler, J., et al. (2019). Topological control of cytokine receptor signaling induces differential effects in hematopoiesis. Science *364*, eaav7532.

Moraga, I., Spangler, J.B., Mendoza, J.L., Gakovic, M., Wehrman, T.S., Krutzik, P., and Garcia, K.C. (2017). Synthekines are surrogate cytokine and growth factor agonists that compel signaling through non-natural receptor dimers. eLife *6*, e22882.

Moraga, I., Wernig, G., Wilmes, S., Gryshkova, V., Richter, C.P., Hong, W.-J., Sinha, R., Guo, F., Fabionar, H., Wehrman, T.S., et al. (2015). Tuning cytokine receptor signaling by re-orienting dimer geometry with surrogate ligands. Cell *160*, 1196–1208.

Morin, A., Eisenbraun, B., Key, J., Sanschagrin, P.C., Timony, M.A., Ottaviano, M., and Sliz, P. (2013). Collaboration gets the most out of software. eLife *2*, e01456.

Ng, C.T., Mendoza, J.L., Garcia, K.C., and Oldstone, M.B. (2016). Alpha and beta type 1 interferon signaling: passage for diverse biologic outcomes. Cell *164*, 349–352.

Ng, J., and Cantrell, D. (1997). STAT3 is a serine kinase target in T lymphocytes. Interleukin 2 and T cell antigen receptor signals converge upon serine 727. J. Biol. Chem. *272*, 24542–24549.

Ouyang, W., and O'Garra, A. (2019). IL-10 Family cytokines IL-10 and IL-22: from basic science to clinical translation. Immunity *50*, 871–891.

Overwijk, W.W., Tagliaferri, M.A., and Zalevsky, J. (2021). Engineering IL-2 to give new life to T cell immunotherapy. Annu. Rev. Med. *72*, 281–311.

Piehler, J., Thomas, C., Garcia, K.C., and Schreiber, G. (2012). Structural and dynamic determinants of type I interferon receptor assembly and their functional interpretation. Immunol. Rev. *250*, 317–334.

Quigley, M., Huang, X., and Yang, Y. (2008). STAT1 signaling in CD8 T cells is required for their clonal expansion and memory formation following viral infection in vivo. J. Immunol. *180*, 2158–2164.

Ring, A.M., Lin, J.-X., Feng, D., Mitra, S., Rickert, M., Bowman, G.R., Pande, V.S., Li, P., Moraga, I., Spolski, R., et al. (2012). Mechanistic and structural insight into the functional dichotomy between IL-2 and IL-15. Nat. Immunol. *13*, 1187–1195.

Ross, S.H., and Cantrell, D.A. (2018). Signaling and function of interleukin-2 in T lymphocytes. Annu. Rev. Immunol. *36*, 411–443.

Russell, S.M., Johnston, J.A., Noguchi, M., Kawamura, M., Bacon, C.M., Friedmann, M., Berg, M., McVicar, D.W., Witthuhn, B.A., Silvennoinen, O.,

et al. (1994). Interaction of IL-2Rβ and γ_c chains with Jak1 and Jak3: implication for XSCID and XCID. Science *266*, 1042–1045.

Sandler, N.G., Bosinger, S.E., Estes, J.D., Zhu, R.T.R., Tharp, G.K., Boritz, E., Levin, D., Wijeyesinghe, S., Makamdop, K.N., del Prete, G.Q., et al. (2014). Type I interferon responses in rhesus macaques prevent SIV infection and slow disease progression. Nature *511*, 601–605.

Saxton, R.A., Tsutsumi, N., Su, L.L., Abhiraman, G.C., Mohan, K., Henneberg, L.T., Aduri, N.G., Gati, C., and Garcia, K.C. (2021). Structure-based decoupling of the pro- and anti-inflammatory functions of interleukin-10. Science *371*, eabc8433.

Sharma, N., Longjam, G., and Schreiber, G. (2016). Type I interferon signaling is decoupled from specific receptor orientation through lenient requirements of the transmembrane domain. J. Biol. Chem. *291*, 3371–3384.

Shoichet, B.K., and Kobilka, B.K. (2012). Structure-based drug screening for G-protein-coupled receptors. Trends Pharmacol. Sci. *33*, 268–272.

Shourian, M., Beltra, J.-C., Bourdin, B., and Decaluwe, H. (2019). Common gamma chain cytokines and CD8 T cells in cancer. Semin. Immunol. *42*, 101307.

Siegel, A.M., Heimall, J., Freeman, A.F., Hsu, A.P., Brittain, E., Brenchley, J.M., Douek, D.C., Fahle, G.H., Cohen, J.I., Holland, S.M., and Milner, J.D. (2011). A critical role for STAT3 transcription factor signaling in the development and maintenance of human T cell memory. Immunity *35*, 806–818.

Silva, D.-A., Yu, S., Ulge, U.Y., Spangler, J.B., Jude, K.M., Labão-Almeida, C., Ali, L.R., Quijano-Rubio, A., Ruterbusch, M., Leung, I., et al. (2019). De novo design of potent and selective mimics of IL-2 and IL-15. Nature *565*, 186–191.

Smith, J.S., Lefkowitz, R.J., and Rajagopal, S. (2018). Biased signalling: from simple switches to allosteric microprocessors. Nat. Rev. Drug Discov. *17*, 243–260.

Spangler, J.B., Moraga, I., Mendoza, J.L., and Garcia, K.C. (2015). Insights into cytokine-receptor interactions from cytokine engineering. Annu. Rev. Immunol. *33*, 139–167.

Stroud, R.M., and Wells, J.A. (2004). Mechanistic diversity of cytokine receptor signaling across cell membranes. Sci. STKE *2004*, re7.

Subramanian, A., Tamayo, P., Mootha, V.K., Mukherjee, S., Ebert, B.L., Gillette, M.A., Paulovich, A., Pomeroy, S.L., Golub, T.R., Lander, E.S., and Mesirov, J.P. (2005). Gene set enrichment analysis: a knowledge-based approach for interpreting genome-wide expression profiles. Proc. Natl. Acad. Sci. USA *102*, 15545–15550.

Thomas, C., Moraga, I., Levin, D., Krutzik, P.O., Podoplelova, Y., Trejo, A., Lee, C., Yarden, G., Vleck, S.E., Glenn, J.S., et al. (2011). Structural linkage between ligand discrimination and receptor activation by type I interferons. Cell *146*, 621–632.

Walter, T.S., Meier, C., Assenberg, R., Au, K.-F., Ren, J., Verma, A., Nettleship, J.E., Owens, R.J., Stuart, D.I., and Grimes, J.M. (2006). Lysine methylation as a routine rescue strategy for protein crystallization. Structure *14*, 1617–1622.

Wang, C.-I., Brauer, P., Yeo, S.P., Tan, H.C., and Connelly, J.E. (2016). IL2R-beta/common gamma chain antibodies. U.S. Patent 20160367664 A1, filed August 5, 2016, and published December 22, 2016.

Wang, X., Rickert, M., and Garcia, K.C. (2005). Structure of the quaternary complex of interleukin-2 with its alpha, beta, and gammac receptors. Science *310*, 1159–1163.

Wu, Y., Tian, Z., and Wei, H. (2017). Developmental and functional control of natural killer cells by cytokines. Front. Immunol. *8*, 930.

Xue, H.H., Fink, D.W.J., Zhang, X., Qin, J., Turck, C.W., and Leonard, W.J. (2002). Serine phosphorylation of Stat5 proteins in lymphocytes stimulated with IL-2. Int. Immunol. *14*, 1263–1271.

Zhang, H., Yea, K., Xie, J., Ruiz, D., Wilson, I.A., and Lerner, R.A. (2013). Selecting agonists from single cells infected with combinatorial antibody libraries. Chem. Biol. *20*, 734–741.

Please cite this article in press as: Yen et al., Facile discovery of surrogate cytokine agonists, Cell (2022), https://doi.org/10.1016/j.cell.2022.02.025

STAR★METHODS

KEY RESOURCES TABLE

REAGENT or RESOURCE	SOURCE	IDENTIFIER
Antibodies		
Anti-human CD3e	BioLegend	Cat#317326; clone OKT3; RRID: AB_11150592
Anti-human CD28	BioLegend	Cat#302943; clone CD28.2; RRID: AB_2616667
Alexa Fluor 647 Mouse Anti-Stat5 (pY694)	BD Biosciences	Cat#612599; 47/Stat5(pY694); RRID: AB_399882
Mouse Anti-Stat5 (pY694), PE	BD Biosciences	Cat#612567; 47/Stat5(pY694); RRID: AB_399858
Mouse Anti-Stat3 (pY705), Alexa Fluor 647	BD Biosciences	Cat#557815; clone 4/P-STAT3; RRID: AB_647144
Phospho-Stat1 (Tyr701) Rabbit mAb, Alexa Fluor 647 Conjugate	Cell Signaling Technology	Cat#8009S; clone 58D6; RRID: AB_647144
Phospho-Stat1 (Tyr701) Rabbit mAb, Alexa Fluor 488 Conjugate	Cell Signaling Technology	Cat#9174S; clone 58D6; RRID: AB_2198287
Phospho-S6 Ribosomal Protein (Ser240/244) XP Rabbit mAb, Alexa Fluor 488 Conjugate	Cell Signaling Technology	Cat#5018S; clone D68F8; RRID: AB_10695861
HA-Tag Mouse mAb, Alexa Fluor 647 Conjugate	Cell Signaling Technology	Cat#3444S; clone 6E2; RRID: AB_1281296
Ultra-LEAF Purified anti-human CD337 (NKp30) Antibody	BioLegend	Cat#325224; clone P30-15; RRID: AB_2814183
Anti-human CD107a (LAMP-1) Antibody, FITC	Biolegend	Cat#328606; clone H4A3; RRID: AB_1186036
BD GolgiPlug Protein Transport Inhibitor (containing Brefeldin A)	BD Biosciences	Cat#555029; RRID: AB_2869014
GolgiStop Protein Transport Inhibitor (Containing Monensin)	BD Biosciences	Cat#554724; RRID: AB_2869012
Fixation/Permeabilization Solution Kit	BD Biosciences	Cat#554714; RRID: AB_2869008
PE-Cy7 Mouse Anti-Human TNF	BD Biosciences	Cat#557647; clone Mab11; RRID: AB_396764
Perm buffer III	BD Biosciences	Cat#558050; RRID: AB_2869118
Mouse Anti-Human CD8, PE	BD Biosciences	Cat#555635; clone HIT8a; RRID: AB_395997
Mouse Anti-Human MIP-1β, PE	BD Biosciences	Cat#550078; clone D21-1351; RRID: AB_393549
Mouse Anti-Human IFN-γ, Alexa Fluor 647	BD Biosciences	Cat#557729; clone B27; RRID: AB_396837
Anti-human CD122 (IL-2Rβ) Antibody, APC	Biolegend	Cat#339008; clone TU27; RRID: AB_2123575
Anti-human CD3 Antibody, APC	Biolegend	Cat#300439; clone UCHT1; RRID: AB_420948
Anti-human CD45RA Antibody, APC	Biolegend	Cat#304150; clone HI100; RRID: AB_2564158
Anti-human IFN-γ Antibody, APC	Biolegend	Cat#506510; clone B27; RRID: AB_315443
Anti-human CD8 Antibody, APC/Cyanine7	Biolegend	Cat#344714; clone SK1; RRID: AB_2044006
Anti-human CD56 (NCAM) Antibody, Brilliant Violet 605	Biolegend	Cat#362538; clone 5.1H11; RRID: AB_2565856
Anti-human CD197 (CCR7) Antibody, Brilliant Violet 605	Biolegend	Cat#353224; clone G043H7; RRID: AB_2561753
Anti-human CD8a Antibody, Brilliant Violet 605	Biolegend	Cat#344742; clone SK1; RRID: AB_2566513
Anti-human CD4 Antibody, Brilliant Violet 785	Biolegend	Cat#300554; clone RPA-T4; RRID: AB_2564382
Anti-human CD3 Antibody, FITC	Biolegend	Cat#300452; clone UCHT1; RRID: AB_2564148
Anti-human CD4 Antibody, FITC	Biolegend	Cat#300538; clone RPA-T4; RRID: AB_2562052
FITC anti-human CD69 Antibody	Biolegend	Cat#310904; Clone FN50; RRID: AB_314839
Anti-human CD3 Antibody, Pacific Blue	Biolegend	Cat#300431; clone UCHT1; RRID: AB_1595437
Anti-human CD4 Antibody, Pacific Blue	Biolegend	Cat#300521; clone RPA-T4; RRID: AB_493098
Anti-human IL-2 Antibody, Pacific Blue	Biolegend	Cat#500307; clone MQ1-17H12; RRID: AB_315094
Phospho-p44/42 MAPK (Erk1/2) (Thr202/Tyr204) Rabbit mAb, Alexa Fluor 647 Conjugate	Biolegend	Cat#13148s; clone 197G2; RRID: AB_2798131
Phospho-Akt (Ser473) XP Rabbit mAb, Alexa Fluor 647 Conjugate	Cell Signaling Technology	Cat#4075S; clone DE9; RRID: AB_916029

(*Continued on next page*)

Please cite this article in press as: Yen et al., Facile discovery of surrogate cytokine agonists, Cell (2022), https://doi.org/10.1016/j.cell.2022.02.025

Continued

REAGENT or RESOURCE	SOURCE	IDENTIFIER
Bacterial and virus strains		
Mix & Go Competent Cells - DH5α	Zymo Research	Cat#T3007
Biological samples		
Human peripheral mononuclear cells (PBMCs), isolated from leukocyte reduction shuttles	Stanford Blood Center	N/A
Chemicals, peptides, and recombinant proteins		
SA sensor chip	Cytiva	Cat#BR-1005-31
HBS-P	Cytiva	Cat#BR-1006-71
EasySep Magnet	StemCell Technologies	Cat#18000
Human $CD8^+$ T cell Isolation Kit	Miltenyi	Cat#130-096-495
LS magnetic selection column	Miltenyi	Cat#130-042-401
EasySep Human Naïve Pan T Cell Isolation Kit	StemCell Technologies	Cat#17961
ExpiFectamine 293 Transfection Kit	Gibco	Cat#A14525
Sapphire Baculovirus DNA	Allele	Cat#ABP-BVD-10002
RNeasy Plus Mini Kit	Qiagen	Cat#74134
CellTrace Violet Proliferation Kit	Invitrogen	Cat#C34557
Bio-Safe Coomassie G-250 Stain, 5L	Biorad	Cat#1610787
UltraComp eBeads	eBiosciences	Cat#01-2222-42
16% Paraformaldehyde aqueous solution	Electron Microscopy Sciences	Cat#15710
EndoH	Produced in house	N/A
Kifunensine	Toronto Research Chemicals	Cat#K450000
BirA	Produced in house (Fairhead and Howarth, 2015)	N/A
Streptavidin	Sigma	Cat#189730
Alexa Flour 647 C_2 Maleimide	Invitrogen	Cat#A20347
Human MSA-IL-2	Produced in house ((Glassman et al., 2021a)	Produced in house
Human IFNω	Produced in house (Thomas et al., 2011)	Produced in house
Human IL-15	R&D systems	Cat#247-ILB-025
Human IL-7	R&D systems	Cat#207-IL-010
PE-AnnexinV	Biolegend	Cat#640947
Ionomycin	Sigma	Cat#I9657-1MG
Phorbol 12-myristate 13-acetate (PMA)	Sigma	Cat#P8139-5MG
Cellfectin II	Gibco	Cat#10362100
Carboxypeptidase A	Sigma	Cat#C9268
Carboxypeptidase B	Sigma	Cat#217356
Expi293 Expression Medium	Gibco	Cat#A1435101
Sf-900 III Media	Invitrogen	Cat#12658019
ESF 921 Insect Cell Culture Medium	Expression Systems	Cat#96-001-01
MY140-F	This paper	N/A
MY140-R	This paper	N/A
MY141-F	This paper	N/A
MY141-R	This paper	N/A
MY177-F	This paper	N/A
MY177-R	This paper	N/A
MY171-F	This paper	N/A
MY171-R	This paper	N/A
MY144-F	This paper	N/A

(*Continued on next page*)

Please cite this article in press as: Yen et al., Facile discovery of surrogate cytokine agonists, Cell (2022), https://doi.org/10.1016/j.cell.2022.02.025

Continued

REAGENT or RESOURCE	SOURCE	IDENTIFIER
MY144-R	This paper	N/A
MY145-F	This paper	N/A
MY145-R	This paper	N/A
MY178-F	This paper	N/A
MY178-R	This paper	N/A
MY172-F	This paper	N/A
MY172-R	This paper	N/A
MY142-F	This paper	N/A
MY142-R	This paper	N/A
MY143-F	This paper	N/A
MY143-R	This paper	N/A
MY179-F	This paper	N/A
MY179-R	This paper	N/A
MY173-F	This paper	N/A
MY173-R	This paper	N/A
MY188-F	This paper	N/A
MY188-R	This paper	N/A
MY189-F	This paper	N/A
MY189-R	This paper	N/A
MY190-F	This paper	N/A
MY190-R	This paper	N/A
MY191-F	This paper	N/A
MY191-R	This paper	N/A
MY192-F	This paper	N/A
MY192-R	This paper	N/A
MY193-F	This paper	N/A
MY193-R	This paper	N/A
MY194-F	This paper	N/A
MY194-R	This paper	N/A
MY195-F	This paper	N/A
MY195-R	This paper	N/A
IL2Rβ-VHH6	This paper	N/A
γ_c-VHH6	This paper	N/A
Human IL2Rβ ECD	This paper	N/A
Human γ_c ECD	This paper	N/A
HIS1	This paper	N/A
HIS2	This paper	N/A
HIS3	This paper	N/A
HIS4	This paper	N/A
HIS5	This paper	N/A
HIS6	This paper	N/A
HIS7	This paper	N/A
A1 VHH monomer	This paper	N/A
10Rβ1-2Rβ6 (8a.a. linker)	This paper	N/A
10Rβ3-2Rβ6 (8a.a. linker)	This paper	N/A
10Rβ4-2Rβ1 (8a.a. linker)	This paper	N/A
2Rβ3-10Rβ1 (8a.a. linker)	This paper	N/A
10Rβ1-2Rβ6 (0a.a. linker)	This paper	N/A
10Rβ1-2Rβ6 (4a.a. linker)	This paper	N/A
10Rβ1-2Rβ6 (12a.a. linker)	This paper	N/A

(*Continued on next page*)

Please cite this article in press as: Yen et al., Facile discovery of surrogate cytokine agonists, Cell (2022), https://doi.org/10.1016/j.cell.2022.02.025

Continued

REAGENT or RESOURCE	SOURCE	IDENTIFIER
10Rβ1-2Rβ6 (16a.a. linker)	This paper	N/A
10Rβ1-2Rβ6-Fc	This paper	N/A
Critical commercial assays		
Superdex 200 Increase column 10/300 GL	Cytiva	Cat#28990944
Superdex 75 Increase column 10/300 GL	Cytiva	Cat#29148721
SA sensor chip	Cytiva	Cat#BR-1005-31
HBS-P	Cytiva	Cat#BR-1006-71
Yeast-Display Nanobody Library (NbLib)	Kerafast	Cat#EF0014-FP
Deposited data		
γ_c:γ_c-VHH6 Complex Crystal Structure	RSCB	PDB: 7S2R
RNA-seq dataset	GEO	GEO: GSE183436
IL2Rβ:β-VHH6 Complex Crystal Structure	RSCB	PDB: 7S2S
Experimental models: Cell lines		
Human: Expi293F	GIBCO	Cat#A14527
Insect: *Spodoptera frugiperda* (*Sf9*)	ATCC	Cat#CRL-1711
Insect: *Trichoplusia ni* (*T. ni*)	Expression Systems	Cat#94-002F
Human: YT-1 (CD25+)	Kuziel et al., 1993	N/A
Human: K-562	ATCC	Cat#CCL-243
Human: A-375	ATCC	Cat#CRL-1619
Recombinant DNA		
pD649 MY140-F	This paper	N/A
pD649 MY140-R	This paper	N/A
pD649 MY141-F	This paper	N/A
pD649 MY141-R	This paper	N/A
pD649 MY177-F	This paper	N/A
pD649 MY177-R	This paper	N/A
pD649 MY171-F	This paper	N/A
pD649 MY171-R	This paper	N/A
pD649 MY144-F	This paper	N/A
pD649 MY144-R	This paper	N/A
pD649 MY145-F	This paper	N/A
pD649 MY145-R	This paper	N/A
pD649 MY178-F	This paper	N/A
pD649 MY178-R	This paper	N/A
pD649 MY172-F	This paper	N/A
pD649 MY172-R	This paper	N/A
pD649 MY142-F	This paper	N/A
pD649 MY142-R	This paper	N/A
pD649 MY143-F	This paper	N/A
pD649 MY143-R	This paper	N/A
pD649 MY179-F	This paper	N/A
pD649 MY179-R	This paper	N/A
pD649 MY173-F	This paper	N/A
pD649 MY173-R	This paper	N/A
pD649 MY188-F	This paper	N/A
pD649 MY188-R	This paper	N/A
pD649 MY189-F	This paper	N/A
pD649 MY189-R	This paper	N/A

(*Continued on next page*)

Please cite this article in press as: Yen et al., Facile discovery of surrogate cytokine agonists, Cell (2022), https://doi.org/10.1016/j.cell.2022.02.025

Continued

REAGENT or RESOURCE	SOURCE	IDENTIFIER
pD649 MY190-F	This paper	N/A
pD649 MY190-R	This paper	N/A
pD649 MY191-F	This paper	N/A
pD649 MY191-R	This paper	N/A
pD649 MY192-F	This paper	N/A
pD649 MY192-R	This paper	N/A
pD649 MY193-F	This paper	N/A
pD649 MY193-R	This paper	N/A
pD649 MY194-F	This paper	N/A
pD649 MY194-R	This paper	N/A
pD649 MY195-F	This paper	N/A
pD649 MY195-R	This paper	N/A
pD649 IL2Rβ-Nb6	This paper	N/A
pD649 γ_c-Nb6	This paper	N/A
pD649	ATUM	Cat#PD649
Software and algorithms		
FlowJo v10.5	Tree Star	RRID: SCR_008520
GraphPad Prism 9.1.0	GraphPad Software	RRID: SCR_002798
BIAevaluation software	Cytiva	RRID: SCR_015936
PHENIX	Liebschner et al., 2019	RRID:SCR_014224
Coot	Emsley et al., 2010	RRID:SCR_014222
SBGrid	Morin et al., 2013	RRID:SCR_003511
DESEQ2	Love et al., 2014	RRID:SCR_015687
STAR	https://github.com/alexdobin/STAR/releases	RRID:SCR_004463
UCSF ChimeraX	https://www.cgl.ucsf.edu/chimerax/	RRID:SCR_015872

RESOURCE AVAILABILITY

Lead contact

Further information and requests for resources and reagents should be directed to and will be fulfilled by the lead contact, K. Christopher Garcia (kcgarcia@stanford.edu).

Materials availability

Plasmids generated in this study will be provided by the lead contact upon completion of a Materials Transfer Agreement.

Data and code availability

- RNA-seq data have been deposited at GEO and are publicly available as of the date of publication. Accession numbers are listed in the key resources table.
- Crystallography data have been deposited at RSCB PDB and are publicly available as of the date of publication. PDB IDs are listed in the key resources table.
- This paper does not report original code.

EXPERIMENTAL MODEL AND SUBJECT DETAILS

Cell lines and culture conditions for functional studies

Human PBMC were isolated from LRS chambers (Stanford Blood Center) and cryopreserved until time of use. $CD25^+$ YT-1 cells (Kuziel et al., 1993) and PBMC were maintained at 37°C in a 5% CO_2 humidified chamber, and cultured in complete RPMI medium (RPMIc) containing 10% FBS and supplemented with 25mM HEPES, 2mM pyruvate, 4mM GlutaMAX, non-essential amino acids, and penicillin-streptomycin (all cell culture reagents were purchased from Gibco). Prior to stimulation for pERK and pAkt studies, cells

were starved in serum-free RPMI for 1-2 hours. Primary cells were rested overnight without cytokine before measuring signaling.

Normal human primary bronchial/tracheal epithelial cells were purchased from ATCC (PCS-300-010) and grown in Airway Epithelial Cell Basal Media (ATCC PCS-300-030) supplemented with Bronchial/Tracheal Epithelial Cell Growth Kit components (ATCC PCS-300-040) following manufacturer's instructions. A549 cells were maintained in complete DMEM medium containing 10% FBS and supplemented with 25mM HEPES, 2mM sodium pyruvate, 4mM GlutaMAX, and penicillin-streptomycin. NKL cells were cultured in RPMIc containing 100IU human IL-2, with media and IL-2 changes every other day. All cell lines were maintained at 37°C in a 5% CO_2 humidified incubator.

Cell lines and culture conditions for protein expression

Baculovirus was generated in *Spodoptera frugiperda* (Sf9) cells maintained in Sf-900 III SFM (Gibco) supplemented with 10% FBS (Sigma) and GlutaMAX (Gibco). For insect protein expression, *Trichoplusia ni* (High5, Expression Systems) cells grown in ESF 921 Insect Cell Culture Medium (Expression Systems) were infected with baculovirus. Insect cells were maintained at 27°C at ambient CO_2 with shaking at 120rpm.

Expi293 suspension cells (Thermo Fisher) were maintained in Expi293 Expression Medium on a 120rpm shaking platform at 37°C in a 5% CO_2 humidified incubator. Protein was produced by transient transfection using ExpiFectamine (Thermo Fisher).

METHOD DETAILS

Camel immunization

Human IL-2Rβ ECD (a.a. 27-240), human γ_C ECD (a.a. 23-262), human IL-10Rβ ECD (a.a. 20-220), human IFNAR1 ECD (a.a. 28-436), and IFNAR2 ECD (a.a. 27-243) were expressed as Fc fusions in HEK293F cells and purified by protein A affinity chromatography. Purified receptor ECDs were mixed with Freund's adjuvant, then individually injected into healthy Bactrian camels (*Camelus bactrianus*). After the seventh immunization, antiserum titer reached 1.0×10^5 (indicating a strong immune response) and we collected 100 mL of peripheral blood for phage display library construction. All camel experiments were performed in compliance with ethics guidelines approved by Shanghai Science and Technology Committee (STCSM).

VHH library construction

Following isolation of peripheral blood lymphocytes (PBLs) from immunized camels, RNA was extracted, cDNAs were reverse transcribed, and VHHs were amplified by two-step nested PCR. Purified VHH fragments were subcloned into the phage-display phagemid pMECS and used to construct the phage display libraries. The quality of libraries was evaluated by size and insertion rate. Insertion rate was calculated by randomly screening 24 clones per library and determining insertion size by PCR amplification.

VHH library selection

VHHs specific for IL-2Rβ, γ_C, IL-10Rβ, IFNAR1 (VHH 1, 5, and 6), and IFNAR2 were selected from phage-display libraries using target proteins and enriched by three consecutive rounds of bio-panning with the infection of VCSM13 helper phages. Three hundred individual colonies were randomly selected from the enriched pool and positive clones were identified using periplasmic extract ELISA (PE-ELISA). VHH A1, A5, and A11 were isolated from a yeast-displayed VHH library using standard techniques (Kerafast).

Protein expression

VHH were fused using a 2-8 a.a. linker, and VHH–scFv were fused via an 8 a.a. Gly-Ser linker, unless otherwise indicated. VHH and scFv fusions were cloned into a pD649 mammalian expression vector (ATUM DNA 2.0), which carries an HA secretion signal peptide and a C-terminal 6-His tag. Proteins were expressed in Expi293F cells (Thermo Fisher) for 5-7 days according to manufacturer protocols, isolated using Ni^{2+} affinity chromatography, then further fractionated over a Superdex 200 increase column equilibrated with 20 mM HEPES (pH 7.4) and 150 mM NaCl. The 10Rβ1–2Rβ6 Fc-fusion was isolated using Protein G affinity chromatography (Thermo Fisher), but otherwise processed identically as the other ligands.

RNA-seq experiments

T cells were pre-activated for 4d with α-CD3/CD28, washed, and rested overnight without stimulation. The following day, $CD8^+$ T cells were purified using MACS ($CD8^+$ T cell isolation kit, Miltenyi Biotec), then stimulated with 100nM natural cytokine (hIL-2, hIL-7, hIL-15) or surrogate ligand for 24hr. at 37°C. Total RNA from 1-2 million cells per condition was extracted using an RNeasy micro kit (Qiagen). For each condition, we performed 3 biological replicates, representing samples from 3 independent donors. cDNA library preparation and RNA sequencing were performed by Novogene. cDNA libraries were loaded onto an Illumina NovaSeq 6000 sequencer, PE150 platform. Reference genome and gene model annotation files were downloaded from the genome website browser (NCBI/UCSC/Ensembl) directly. Paired-end clean reads were aligned to the reference genome using STAR software, and differential expression analysis was conducted using the DESeq2 R package (Love et al., 2014). Data (raw and processed) are deposited under GEO accession record GSE183436.

NK experiments

Primary NK cells (from a mixed human PBMC population) were pre-activated for 5-7d with 2μg/mL plate-bound α-NKp30 (Biolegend) with 9nM hIL-15 (R&D) in RPMIc media. Following activation, cells were rested for 1d in RPMIc without stimulation, then plated into

Please cite this article in press as: Yen et al., Facile discovery of surrogate cytokine agonists, Cell (2022), https://doi.org/10.1016/j.cell.2022.02.025

96-well microplates in the presence of hIL-2 or IL-2 surrogate ligands. Media and ligand were refreshed every 3-4d. Cells were analyzed at the indicated time points for cytokine profiling and cytotoxicity.

T cell proliferation

PBMC were pre-activated for 3-4d with 2.5μg/mL plate-bound α-CD3 (clone OKT3, Biolegend) and 5μg/mL soluble α-CD28 (Biolegend), then rested for 1d in RPMIc without stimulation. Cells were loaded with 5uM CellTrace Violet, then plated in 96-well format in media containing 100nM hIL-2 or surrogate ligands. Live $CD4^+$ and $CD8^+$ T cells were enumerated using cell surface antibodies and propidium iodide exclusion after 3-5d in culture.

T cell differentiation

Naïve pan-T cells were isolated to >90% purity from 5-10E+7 cryopreserved PBMCs using an EasySep Human Naïve Pan T Cell Isolation Kit (STEMCELL technologies). Cells were preactivated using 2μg/mL plate-bound α-CD3 (clone OKT3, Biolegend) and 1μg/mL soluble α-CD28 (Biolegend) in RPMIc for 4d. Prior to differentiation, cells were washed and rested in RPMIc without stimulation for 1d, then plated into 96-well microplates with 100nM hIL-2 or IL-2 surrogate ligands. Media and ligand were refreshed after 4d. Cells were analyzed for T memory surface markers or cytokine profiling at 8-10d post differentiation.

Crystallography

For IL-2R VHH crystallography, hIL-2Rβ extracellular domain (a.a. 27-233) and $h\gamma_c$ extracellular domain (a.a. 55-254) were cloned into the pAcGP67a baculoviral vector carrying an N-terminal GP64 signal sequence and C-terminal 6xHis tag. Baculovirus was produced by transfection of Sf9 insect cells with Cellfectin II (Gibco) and Sapphire Baculovirus DNA (Allele) followed by viral amplification in Sf9 cells. Protein was expressed in *T. ni* cells infected for 48-72 h. For γ_c expression, cells were infected in the presence of the endoplasmic reticulum mannosidase I (ERM1) inhibitor, kifunensine (Toronto Research Chemicals). Protein was purified by Ni-NTA affinity chromatography followed by size exclusion chromatography (SEC) using a Superdex S75 increase column (Cytiva). For VHH expression, sequences were cloned into the pD649 vector with an N-terminal HA signal peptide and C-terminal AviTag and 6xHis tag. VHH were expressed by transient transfection in Expi293F cells (Gibco) using an ExpiFectamine 293 Transfection Kit (Gibco) according to manufacturer's protocols. VHH were purified by Ni-NTA affinity chromatography and S75 SEC.

For γ_c:γ_c-VHH6 crystallography, γ_c and γ_c-VHH6 were complexed for 4 hours at 4°C in the presence of carboxypeptidase A (Sigma), carboxypeptidase B (Sigma), and endoglycosidase H (EndoH) in HBS, pH6.8. The complex was purified by S75 SEC and concentrated to 12.9mg/mL. Crystals were grown in a solution of 2M ammonium sulfate, 0.2M BIS-Tris pH5.5 and flash cooled in liquid nitrogen with the addition of 30% glycerol as cryoprotectant. Diffraction data were collected at Stanford Linear Accelerator SSRL beamline 12-1. Data were indexed, integrated, and scaled using the XDS package (Kabsch, 2010). The structure was solved by molecular replacement using PHASER with $h\gamma_c$ (PDB: 2B5I) (Wang et al., 2005) and a VHH with loop deletions (PDB: 5LHR) (Kromann-Hansen et al., 2017). The final model was built by iterative rounds of model building in COOT (Emsley et al., 2010) and refinement in PHENIX (Liebschner et al., 2019). All crystallographic software was installed and configured by SBGrid (Morin et al., 2013).

For IL-2Rβ crystallography, IL-2Rβ and IL-2Rβ-VHH6 were methylated with borane dimethylamine complex (Sigma) and paraformaldehyde (Electron Microscopy Sciences) overnight at 4°C according to previously established protocols (Walter et al., 2006) in the presence of carboxypeptidase A and B (Sigma). The following morning, the reaction was quenched with 200mM Tris pH8.0 and purified by S75 SEC. The complex was concentrated to 11.7mg/mL and crystallized in a solution of 0.23M ammonium sulfate, 0.08M BisTris pH5.5 and 23% PEG3350. Crystals were cryoprotected with 20% PEG 400 and flash cooled in liquid nitrogen. Diffraction data were collected at Stanford Linear Accelerator (SSRL 12-2) and processed as described for the γ_c structure other than that molecular replacement was performed with IL-2Rβ (PDB: 2B5I) (Wang et al., 2005).

For both structures, data refinement and statistics can be found in Table S1 and were deposited in the RSCB protein databank with accession codes PDB: 7S2R (γ_c:γ_c-VHH6) and PDB: 7S2S (IL-2Rβ:β-VHH6).

qRT-PCR

RNA was extracted with an RNeasy Plus kit (QIAGEN), converted to cDNA by a RT-PCR reaction (iSCRIPT reverse transcription kit, Bio-rad), and ISG induction relative to the untreated controls and normalized to GAPDH levels were measured by the PowerTrack SYBR green qPCR assay system (Thermo Fisher Scientific) on a StepOnePlus instrument (Thermo Fisher Scientific). Primer pairs used for transcript amplification are listed in Table S2.

Anti-proliferative activity assay

Human primary bronchial/tracheal epithelial cells were seeded at 1,000 cells/well in 96-well plates. The following day media was replaced with surrogate ligand or IFNω containing media. 3 days post IFN treatment cell density was measured using CellTiter-Glo (Promega) according to the manufacturer's protocol.

A549-hACE2 SARS-CoV-2 antiviral assay

96-well plates were seeded with 20,000 A549-hACE2 cells/well. A549 is a human lung epithelial cell line stably expressing the SARS-CoV-2 receptor, hACE2, to facilitate efficient infection for antiviral assays (Hou et al., 2020a). Culture medium was removed 24 hr.

Please cite this article in press as: Yen et al., Facile discovery of surrogate cytokine agonists, Cell (2022), https://doi.org/10.1016/j.cell.2022.02.025

post-seeding, and a 9-point agonist dose-response (top concentration 1000nM, 10-fold steps) was prepared in "infection medium" (DMEM (Gibco), 5% fetal bovine serum (Hyclone), 1x anti/anti (antibiotic, antimycotic, Gibco). Cells were transported to Biosafety Level 3 after 24hr. treatment with agonists, at which point cells were infected with recombinant SARS-CoV-2 engineered to express nanoluciferase at a multiplicity of infection of 0.25. After incubation for 1hr. at 37°C, input virus was removed, cells were washed once with infection medium and 100μL fresh infection medium was added. As a positive control, a similar dose-response of recombinant human IFNω was employed. As a negative control, the monomeric hIFNAR1-specific VHH "A1" was employed, which should not facilitate the dimerization of the type I interferon receptor subunits. After 48hr. of infection, levels of virus replication were measured by Promega NanoGlo assay measured on a Promega GloMax Luminometer. Similarly treated uninfected sister plates were generated in order to gauge potential cytotoxicity.

SARS-CoV-2 viral inhibition assay

Primary human airway epithelial cells were treated with varying concentrations of HIS ligands, human IFNω positive control, or "A1" VHH monomer negative control for 24hr. prior to infection with SARS-CoV-2 (Washington 1 strain) at a multiplicity of infection of 0.1. After 3d, apical washes were performed to measure viral titer.

NK and NKL functional assays

NK cells were stimulated with hIL-18 (100 ng/mL, R&D), hIL-15 (20 ng/mL, R&D), and hIL-12 (10 ng/mL, BioLegend) for 18hr, washed 3 times, then cultured in cRPMI for 2 days.

NKL cells were rested in cytokine-free media for 2 days. The rested NKL cells were preincubated with 100nM surrogate ligand or hIL-2 for 12h. K562 cells were labeled with 15μM Calcein-AM (BioLegend) for 30min at 37°C. The NKL cells were cocultured with 10,000 K562 cells at indicated effector:target ratios for 4h at 37°C in V bottom 96 well plate. The supernatants were transferred to a new 96 well plate and measured using a Spectramax Gemini dual-scanning microplate (excitation filter: 485 ± 9 nm; band-pass filter: 530 ± 9 nm).

For degranulation and activation of NKL or primary NK cells, cells were rested and pre-stimulated with surrogate agonists for 12h. K562 cells were labeled with 1uM CellTrace Violet (Thermo Fisher) for 20min at 37°C. NK cells were co-cultured with K562 cells for 4h in the presence of FITC-CD107 antibody (BioLegend), GolgiStop and GolgiPlug (BD). The cells were surface stained with NK markers and CD69 antibody for 30min. on ice. IFNγ staining was performed by following the intracellular staining protocol (Invitrogen). The samples were analyzed via flow cytometry.

QUANTIFICATION AND STATISTICAL ANALYSIS

SPR data was analyzed using BIAevaluation software (Cytiva). Flow cytometry data was analyzed using FlowJo software (BD). Statistical analyses were performed using Prism v9 (GraphPad Software). Statistics were determined using Prism v9.1.0 (GraphPad Software). For Figures 7 and S7, one-way ANOVA followed by Dunnett's multiple comparisons tests was used to analyze experiments with more than two groups. For Figure S6E, statistics were calculated using two-way ANOVA followed by Tukey's multiple comparisons tests. Significance is indicated as follows: *$p < 0.05$; **$p < 0.01$; ***$p < 0.001$, ****$p<0.0001$. Data are expressed as mean ± standard deviation of duplicate or triplicate wells, as indicated in the figure legends. Data are representative of two or more independent experiments, except for Figure S6E, which was performed once.

Supplemental figures

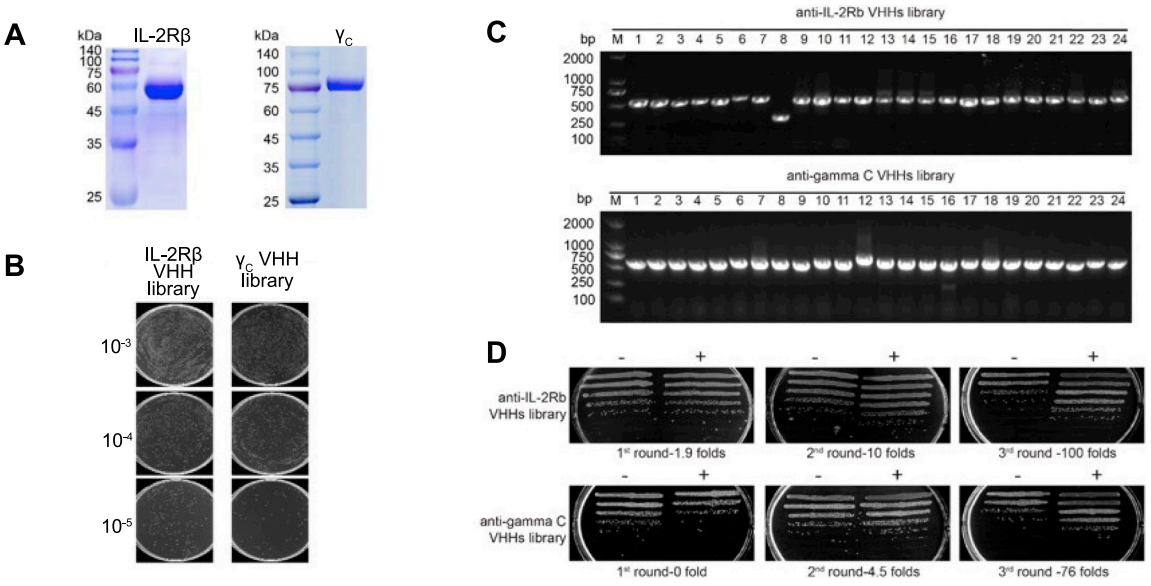

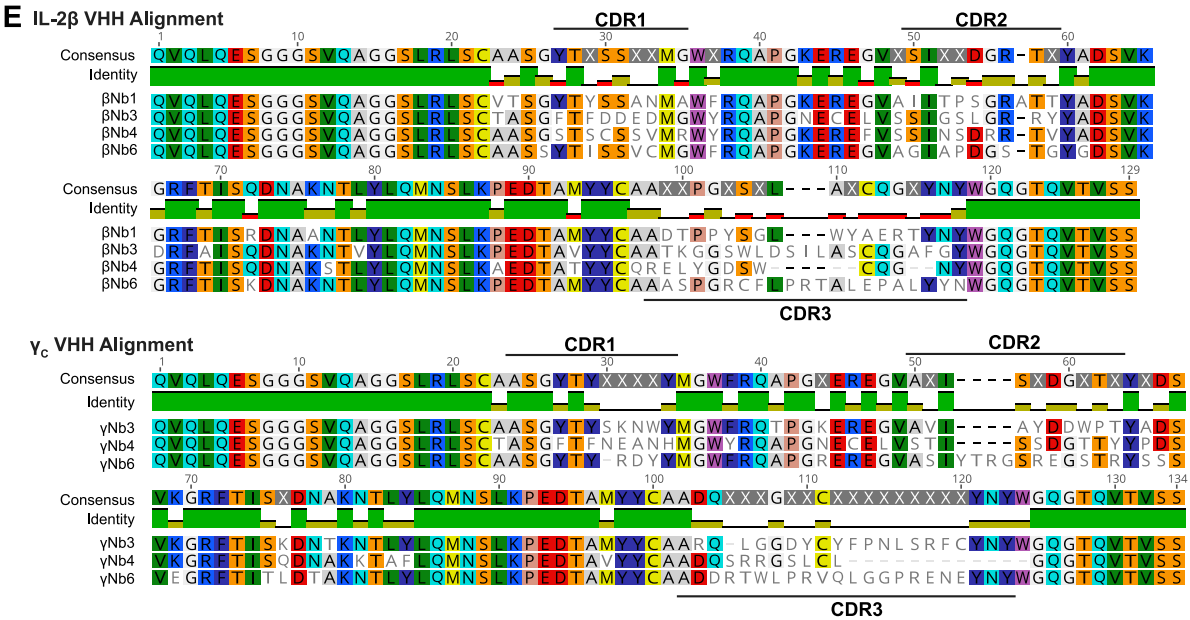

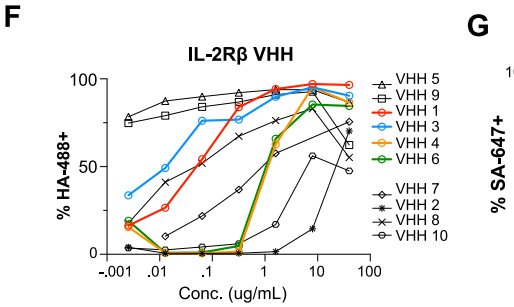

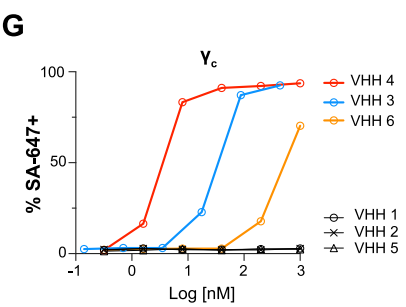

H

VHH / scFv	K_D (nM)
β VHH 1	11
β VHH 3	20
β VHH 4	123
β VHH 6	25
γ VHH 3	7
γ VHH 4	20
γ VHH 6	69
γ scFv1 (P1A3)	145
γ scFv2 (P2B9	79

(legend on next page)

Figure S1. Phage library selection and cell surface screening of VHHs specific for IL-2Rβ and γ_C, related to Figure 1

(A) SDS-PAGE of purified human IL-2Rβ (ECD)-Fc and γ_C (ECD)-Fc antigen used for camel immunization.

(B) Phage library sizes were determined by counting the number of colonies after serial dilution onto plates containing selective antibiotics.

(C) Insertion rate of the libraries measured by PCR of 24 randomly selected clones yielded correct insert rates of 95.8% and 100% for IL-2Rβ and γ_C libraries, respectively.

(D) Enrichment following each round of bio-panning.

(E) Sequence alignment of selected IL-2Rβ- and γ_C-VHH clones used for cell-based receptor-binding assays.

(F) Cell-surface-based screening of IL-2Rβ-specific VHH candidates. YT-1 cells were incubated with varying concentration of HA-tagged VHH, washed, and stained with anti-HA-AlexaFluor488, then analyzed via flow cytometry.

(G) Cell surface screening of γ_C-specific VHH candidates. YT-1 cells were incubated with biotinylated VHH, washed, then stained with streptavidin-AlexaFluor647 followed by detection using flow cytometry.

(H) Steady-state binding affinities between VHH/scFv and IL-2R, as determined by SPR. Values for scFv affinities are derived from patent US20160367664A1 (Wang et al., 2016).

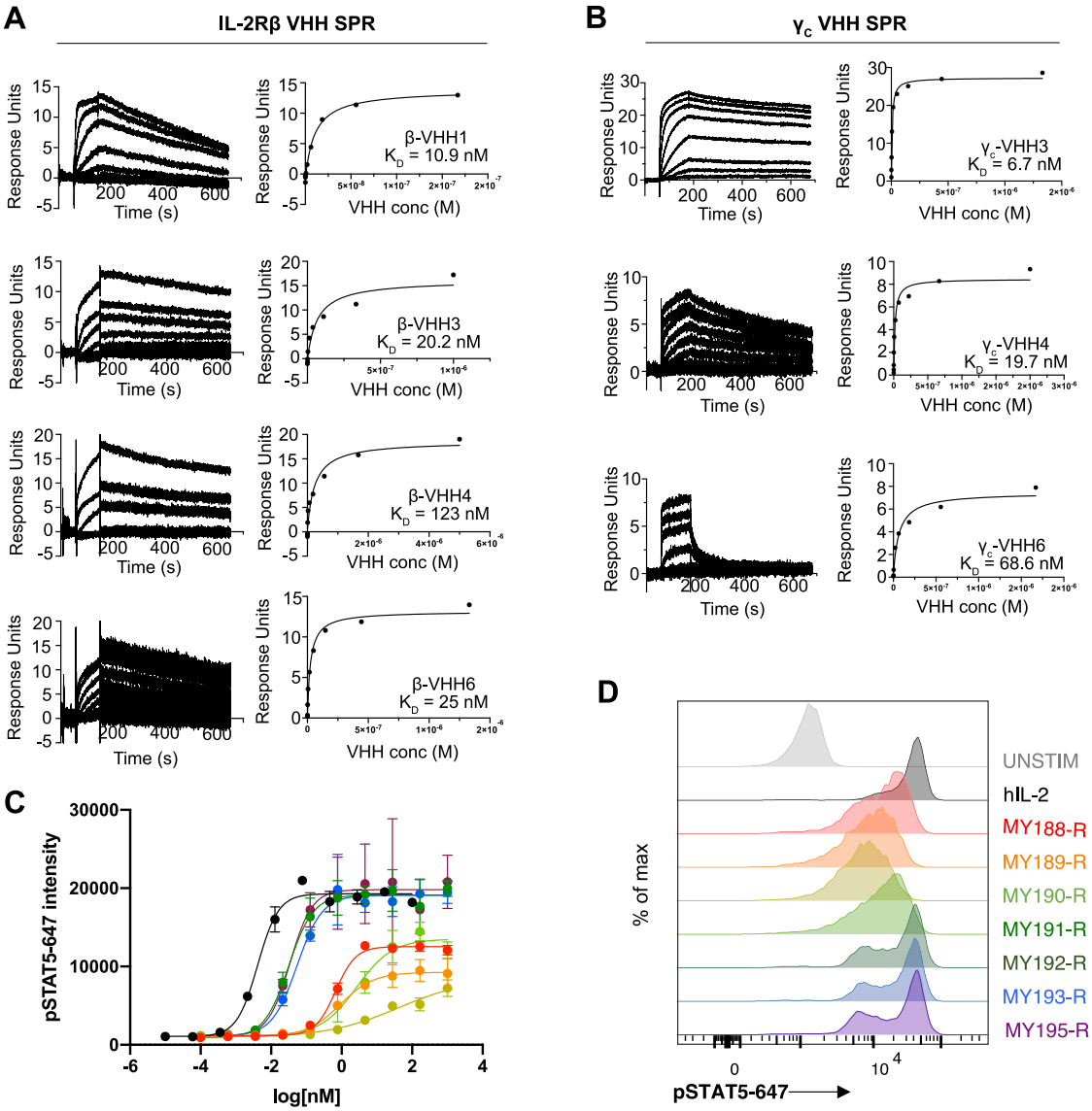

E

		IL2Rβ - γc orientation				IL2Rβ - γc orientation			
		VHH IL2Rβ binder				VHH IL2Rβ binder			
		VHH1	VHH3	VHH4	VHH6	VHH1	VHH3	VHH4	VHH6
VHH γc Binder	VHH3	0 MY140-F	0.63 MY141-F	0 MY177-F	0.02 MY171-F	0.66 MY140-R	0.72 MY141-R	0 MY177-R	1.45 MY171-R
	VHH4	0.37 MY144-F	0.95 MY145-F	0.46 MY178-F	1.05 MY172-F	0.01 MY144-R	0.93 MY145-R	0.02 MY178-R	1.43 MY172-R
	VHH6	.01 MY142-F	0.79 MY143-F	0.45 MY179-F	0.97 MY173-F	0.96 MY142-R	0.86 MY143-R	0.03 MY179-R	1.75 MY173-R
scFv γc	scFv1	0 MY188-F	0.9 MY189-F	1 MY190-F	0 MY191-F	0.62 MY188-R	0.46 MY189-R	0.34 MY190-R	0.73 MY191-R
	scFv2	0 MY192-F	1 MY193-F	0.95 MY194-F	0 MY195-F	1 MY192-R	0.99 MY193-R	1 MY194-R	1 MY195-R

Figure S2. SPR validation of IL-2Rβ- and γC-VHHs and agonist screening in YT-1 cells, related to Figure 1

(A) Biotinylated human IL-2Rβ ECD was immobilized on a streptavidin (SA) sensor chip, and varying concentrations of IL-2Rβ VHH were applied to determine binding parameters using SPR. Sensorgrams are shown on the left, and steady-state binding is plotted on the right. Binding affinities (K_D) were determined by fitting to steady-state response values.

(legend continued on next page)

(B) Biotinylated human γ_C ECD was immobilized on a SA chip, and varying concentrations of γ_C VHH were flowed over the chip to determine binding. Sensorgrams (left) and steady-state binding (right) are displayed as in (A).
(C) Dose-response relationship of pSTAT5 geometric mean flurorescence intensities (gMFI) of selected agonists.
(D) Corresponding histograms showing STAT5 activity in YT-1 cells treated with human IL-2 versus IL-2 surrogate agonists at saturating concentration.
(E) Table shows E_{max} values of all 40 surrogate agonists. E_{max} was baseline subtracted from the unstimulated values and then normalized to that of hIL-2.

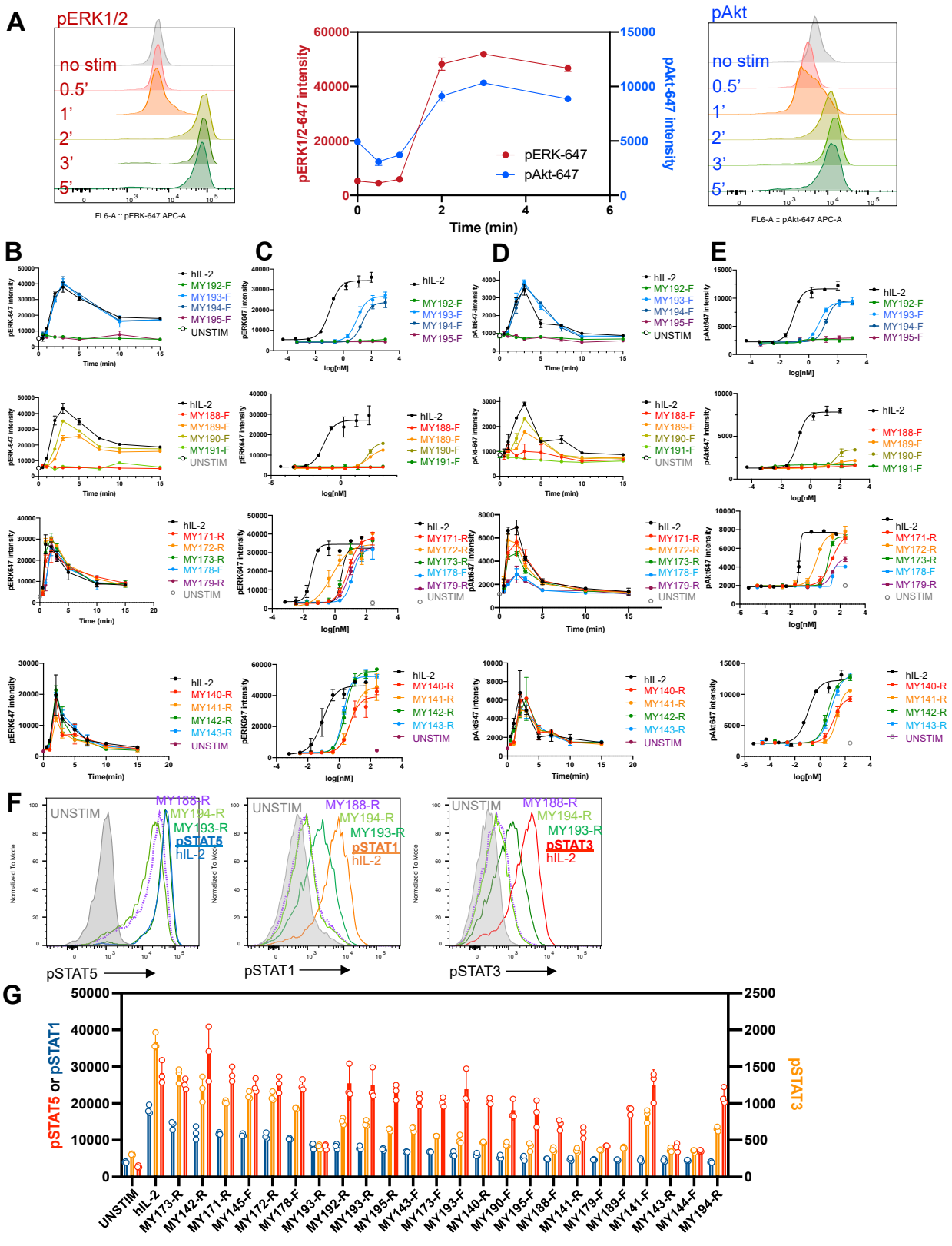

(legend on next page)

Figure S3. Signaling properties of IL-2 surrogate agonists on YT-1 and primary human T cells, related to Figure 2

(A) Kinetics of pERK (left) and pAkt activation (right) in YT-1 cells stimulated with high dose (25 nM) hIL-2. Geometric mean fluorescence intensity (gMFI) of replicate wells was averaged and plotted as a function of time (middle). Phosphorylation peaks by 3 min after stimulation.

(B and D) Time course of pERK activation by hIL-2 (black) versus IL-2 surrogate ligands (colored lines).

(C and E) Dose-response of pERK activation at 3 min post-ligand addition.

(F) Histograms for hIL-2 and selected agonists showing STAT5 (left), STAT1 (middle), and STAT3 (right) activity levels in pre-activated human T cells stimulated with 100-nM ligand.

(G) Pre-activated human T cells were stimulated as in (F), and the gMFI of STAT5, STAT1, or STAT3 antibody staining was plotted as indicated. To aid comparison, these raw data were baseline subtracted with the "unstimulated" values, then normalized to hIL-2 STAT levels in main Figure 2.

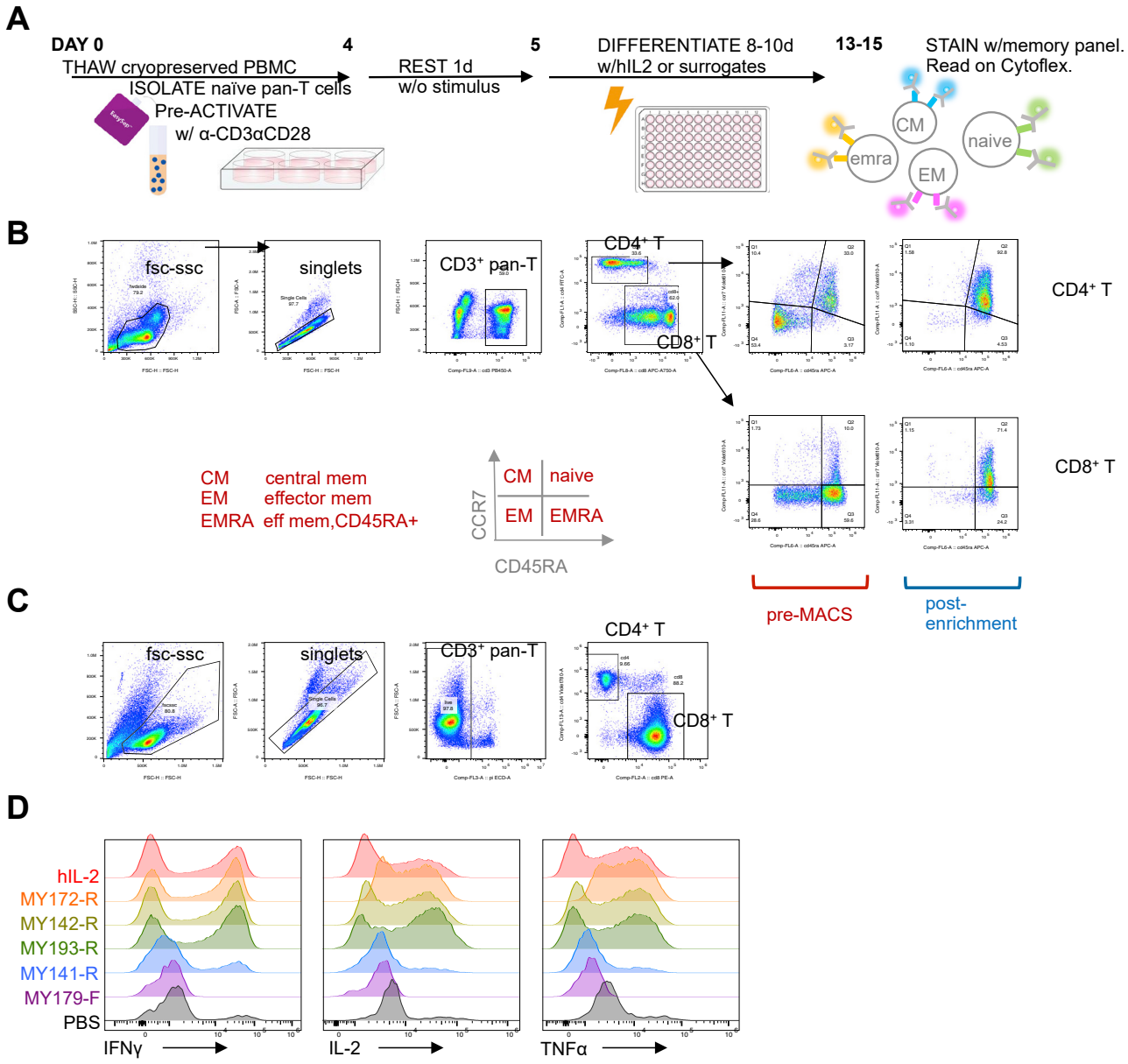

Figure S4. IL-2 surrogate agonists direct differentiation of CD8⁺ T cell memory, related to Figure 5

(A) Schematic outline of human T cell differentiation assay.

(B) Gating scheme for distinguishing CD4⁺ and CD8⁺ memory cell subsets, and example T cell "input" after purification of naive T cells ("post-enrichment").

(C) Gating scheme to distinguish CD4⁺ and CD8⁺ T cells for cytokine profiling.

(D) Example intracellular cytokine staining histograms showing expression of effector cytokines induced by surrogate agonists, as described in (A).

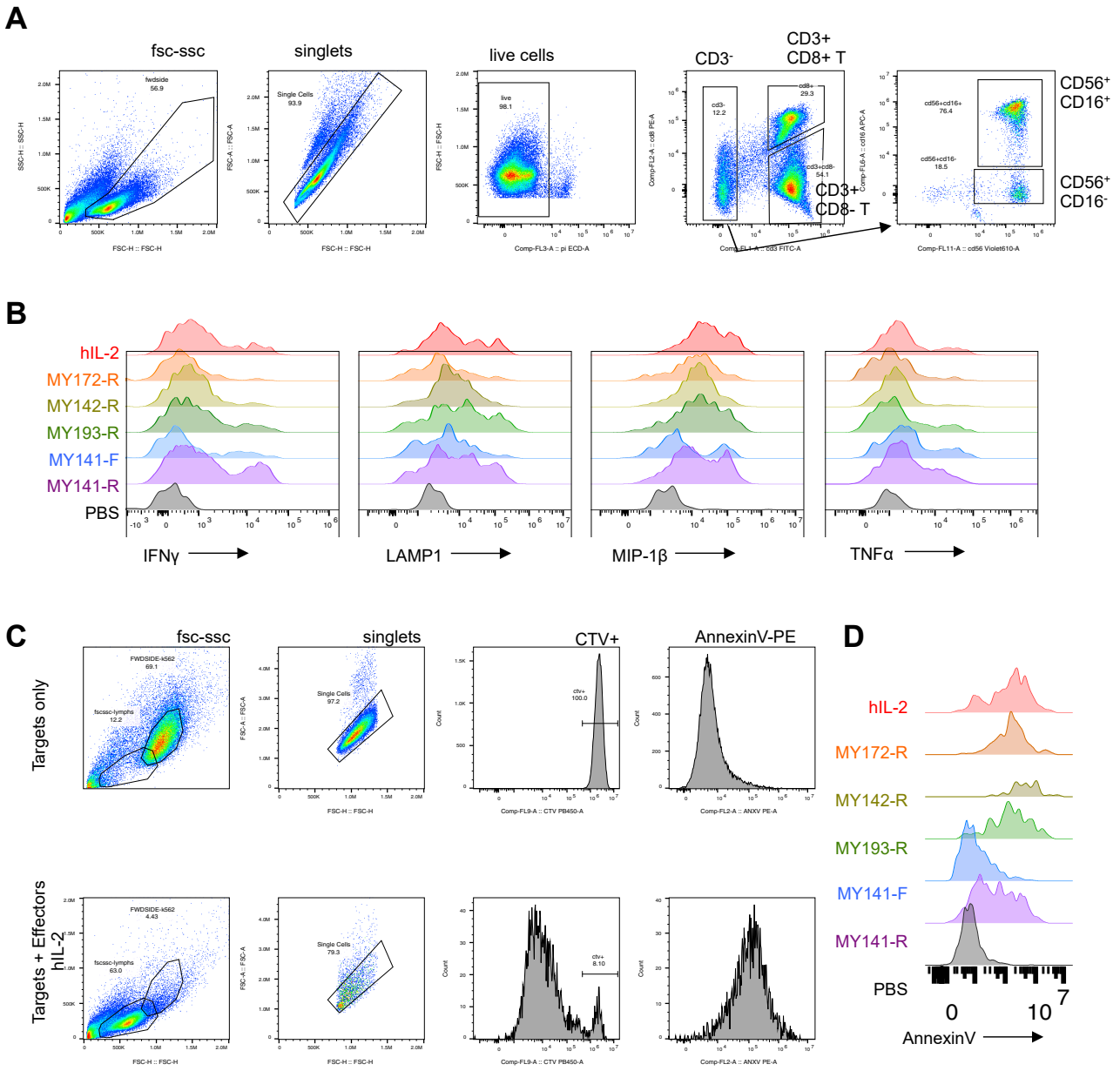

Figure S5. IL-2 surrogate agonists support NK cell proliferation and cytolysis, related to Figure 5

(A) Gating scheme for enumerating T cell versus NK cell types based on cell surface staining.

(B) Histograms displaying NK cell intracellular cytokine staining for hIL-2 or surrogate agonist-cultured cells.

(C) Gating scheme used to identify CTV-loaded target cells and quantify annexin V positivity. Top row shows a well containing target cells only, bottom row contains a mixture of NK effectors + target cells.

(D) Histogram of target cell annexin V staining when mixed with NK cells cultured with 10-nM hIL-2 versus selected IL-2 analogs.

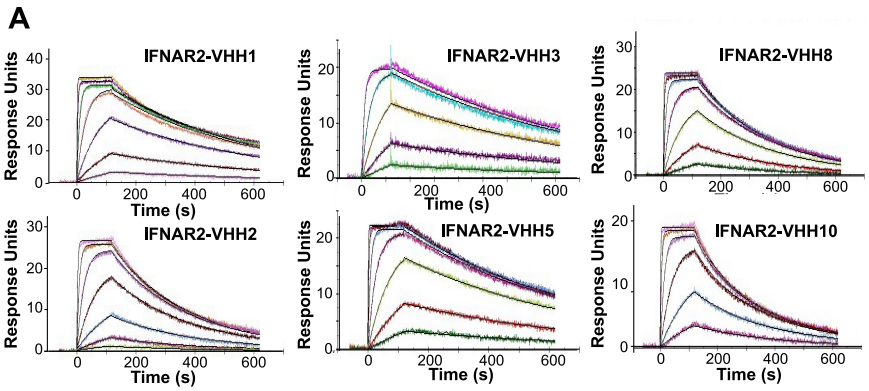

B

IFNAR2 VHH	Binding constants (from kinetic fits)		
	K_D (nM)	K_a	K_d
VHH1	0.31	6.75e+6	2.1e-3
VHH2	0.78	5.52e+6	4.3e-3
VHH3	0.21	5.5e+6	1.2e-3
VHH5	0.23	7.2e+6	1.7e-3
VHH8	0.54	7.5e+6	4.1e-3
VHH10	0.33	1.9e+7	6.2e-3

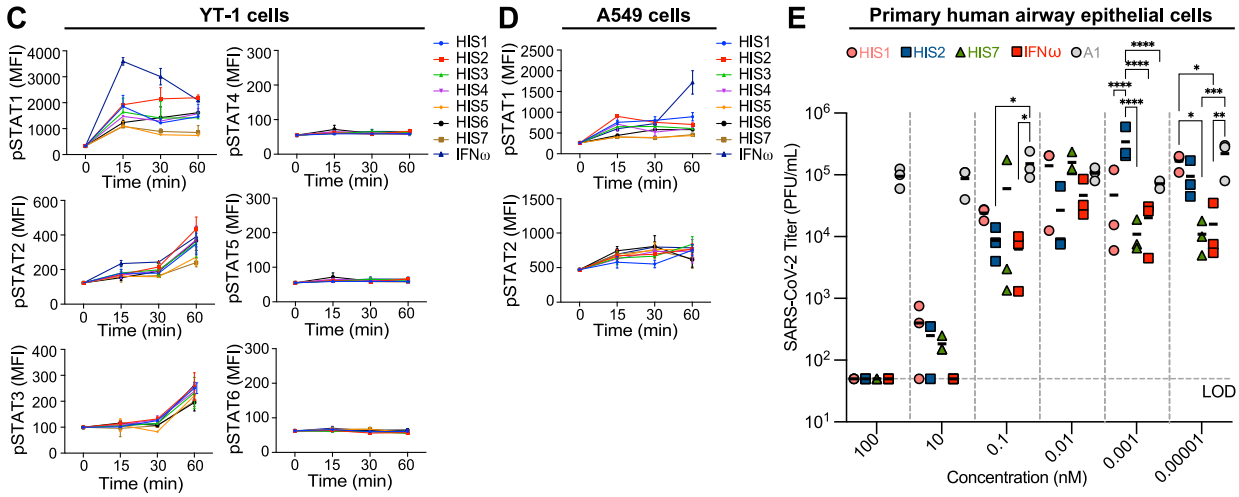

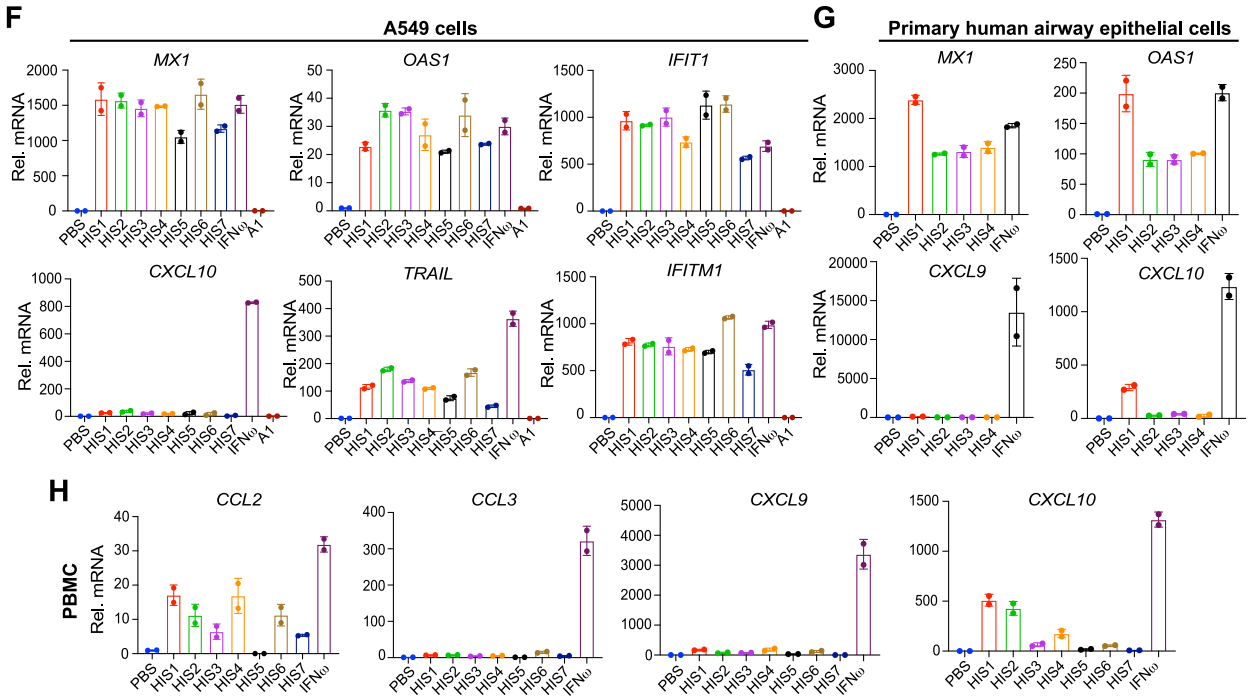

(legend on next page)

Figure S6. Signaling kinetics and gene expression driven by type-I interferon surrogate ligands, related to Figure 6

(A and B) (A) SPR sensorgrams displaying dose-dependent binding of IFNAR2 VHHs to immobilized human IFNAR2 ECD. SPR experiments were performed using the same conditions as for IL-2 specific VHHs (Figure S2). Binding constants were determined from kinetic fitting and summarized in (B).

(C) Kinetics of STAT1-STAT6 phosphorylation induced by surrogate ligands or IFNω in YT-1 cells. YT-1 cells were serum-starved for 1–2 h, then stimulated with 10-nM ligand for 15–60 min at 37°C, fixed and permeabilized, then stained with fluorescently conjugated phospho-antibodies before reading on a flow cytometer.

(D) STAT1 and STAT2 phosphorylation induced by HIS or IFNω at different time points in A549 cells.

(E) SARS-CoV-2 antiviral assay on primary human airway epithelial cells. Cells were pre-treated with HIS, IFNω, or VHH monomer "A1" for 24 h prior to infection with SARS-CoV-2 infection (MOI = 0.1). Viral titers were quantified from apical washes collected at 72 h post-infection. Statistics were calculated using two-way ANOVA followed by Tukey's multiple comparisons tests. Significance is indicated as follows: *$p < 0.05$; **$p < 0.01$; ***$p < 0.001$, ****$p<0.0001$.

(F–H) qRT-PCR analysis of ISG transcripts induced by 10-nM HIS or IFNω for 8 h in (F) A549 cells, (G) primary human airway epithelial cells, or (H) human PBMCs. Data were collected in duplicate and displayed as means with ranges.

A

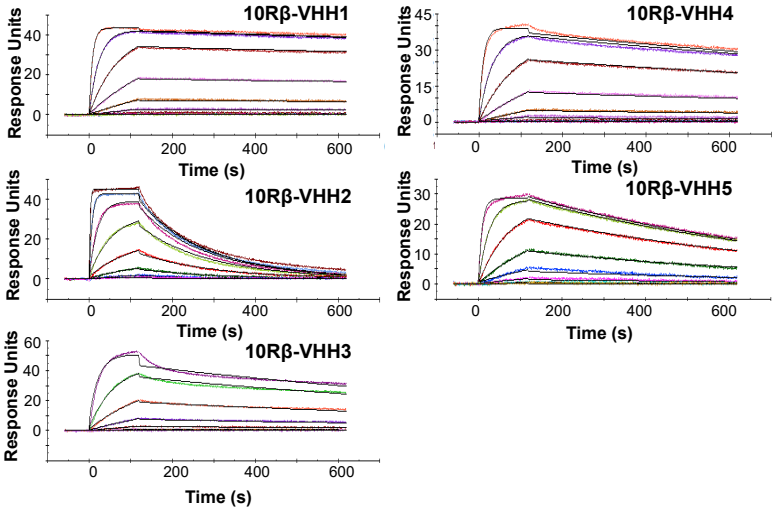

B

IL-10Rβ VHH	Binding constants (from kinetic fits)		
	K_D (nM)	K_a	K_d
VHH1	1.6	9.5e+4	1.5e-4
VHH2	2.2	3.2e+6	7.0e-3
VHH3	2.5	3.0e+5	7.6e-4
VHH4	2.2	2.1e+5	4.7e-4
VHH5	1.7	7.8e+5	1.3e-3

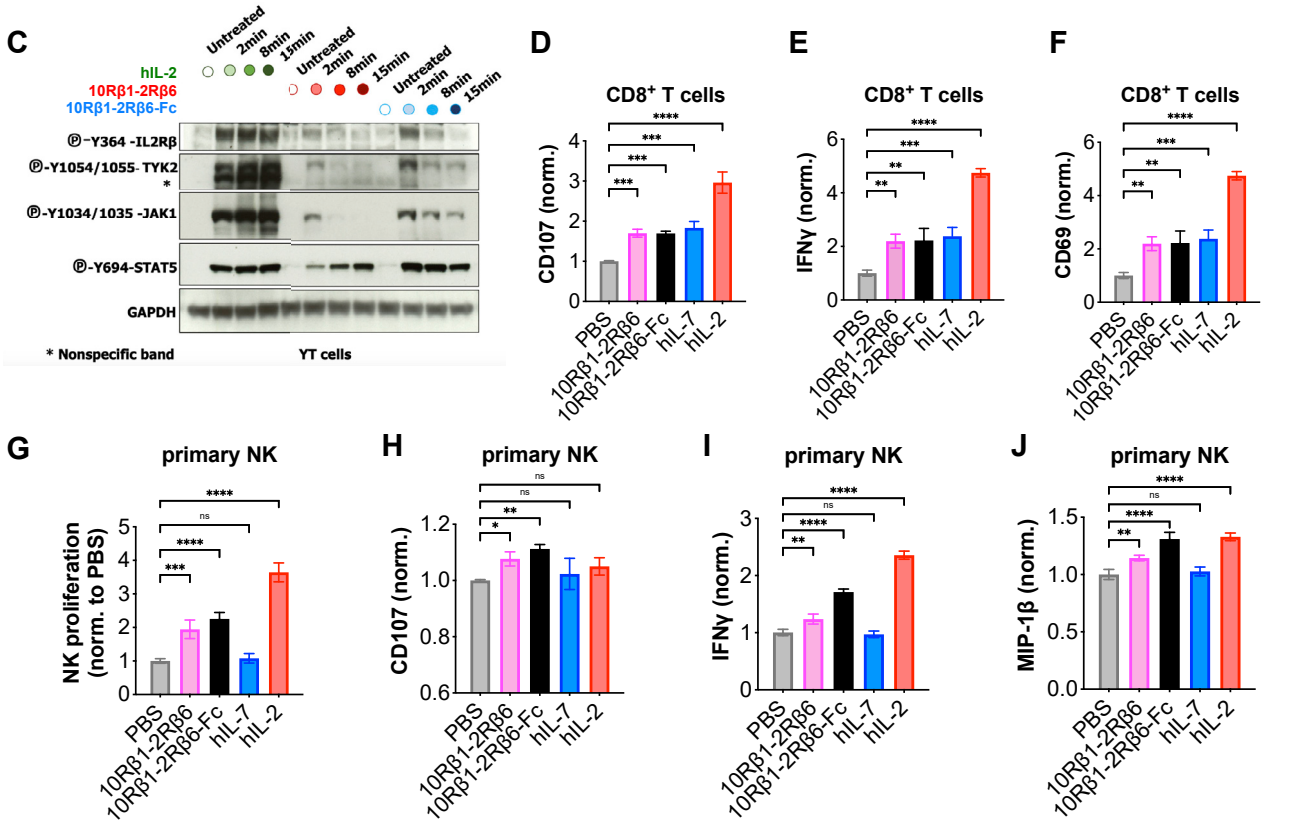

Figure S7. A surrogate agonist compels heterodimerization of IL-2Rβ and IL-10Rβ and shows bias for CD8⁺ T and NK cells, related to Figure 7

(A and B) (A) SPR sensorgrams displaying dose-dependent binding of IL-10Rβ VHHs to immobilized human IL-10Rβ ECD. SPR experiments were performed using the same conditions as for IL-2 specific VHHs (Figure S2). Binding constants were determined from kinetic fitting and summarized in (B).

(C) Proximal signaling of monomeric or Fc-linked 10Rβ1-2Rβ6 surrogate agonist versus hIL-2, assessed by western blotting. YT-1 cells were treated with 100-nM ligand for varying times, lysed, then examined for phosphorylation of IL-2Rβ, TYK2, JAK1, and STAT5.

(D–F) Degranulation and activation of A3A-TCR⁺CD8⁺ T cells in response to monomeric or Fc-linked 10Rβ1-2Rβ6, hIL-7, and hIL-2.

(G–J) Functional properties of monomeric or Fc-linked 10Rβ1-2Rβ6 on primary human NK cells. Human NK cells were treated with surrogate agonists, hIL-7, or hIL-2, then assayed for (G) proliferation or expression of (H) CD107, (I) IFNγ, or (J) MIP-1β. For (D–J), statistics were calculated using one-way ANOVA followed by Dunnett's multiple comparisons tests, with significance indicated follows: *p < 0.05; **p < 0.01; ***p < 0.001, ****p<0.0001.